JGP Journal of General Physiology

RESEARCH ARTICLE

Facilitation of I_{Kr} current by some hERG channel blockers suppresses early afterdepolarizations

Kazuharu Furutani[1,2,3*], Kunichika Tsumoto[1,4*], I-Shan Chen[1], Kenichiro Handa[1], Yuko Yamakawa[1], Jon T. Sack[3], and Yoshihisa Kurachi[1,2]

Drug-induced block of the cardiac rapid delayed rectifying potassium current (I_{Kr}), carried by the human ether-a-go-go-related gene (hERG) channel, is the most common cause of acquired long QT syndrome. Indeed, some, but not all, drugs that block hERG channels cause fatal cardiac arrhythmias. However, there is no clear method to distinguish between drugs that cause deadly arrhythmias and those that are clinically safe. Here we propose a mechanism that could explain why certain clinically used hERG blockers are less proarrhythmic than others. We demonstrate that several drugs that block hERG channels, but have favorable cardiac safety profiles, also evoke another effect; they facilitate the hERG current amplitude in response to low-voltage depolarization. To investigate how hERG facilitation impacts cardiac safety, we develop computational models of I_{Kr} block with and without this facilitation. We constrain the models using data from voltage clamp recordings of hERG block and facilitation by nifekalant, a safe class III antiarrhythmic agent. Human ventricular action potential simulations demonstrate the ability of nifekalant to suppress ectopic excitations, with or without facilitation. Without facilitation, excessive I_{Kr} block evokes early afterdepolarizations, which cause lethal arrhythmias. When facilitation is introduced, early afterdepolarizations are prevented at the same degree of block. Facilitation appears to prevent early afterdepolarizations by increasing I_{Kr} during the repolarization phase of action potentials. We empirically test this prediction in isolated rabbit ventricular myocytes and find that action potential prolongation with nifekalant is less likely to induce early afterdepolarization than action potential prolongation with dofetilide, a hERG channel blocker that does not induce facilitation. Our data suggest that hERG channel blockers that induce facilitation increase the repolarization reserve of cardiac myocytes, rendering them less likely to trigger lethal ventricular arrhythmias.

Introduction

A rapid component of the delayed-rectifier potassium current (I_{Kr}) plays an important role in the repolarization of the cardiac action potential (AP). I_{Kr} is especially important in ventricular muscle of the hearts of large mammals. Certain blockers of I_{Kr} are class III antiarrhythmic agents, used to treat ventricular tachyarrhythmias (Sanguinetti and Jurkiewicz, 1990; Vaughan Williams, 1992; Zeng et al., 1995; Clancy et al., 2003). Blockers of I_{Kr} prolong the AP duration (APD) and effective refractory period to suppress premature ventricular contraction. Blockade of I_{Kr} also is a side effect of many drugs. Blockers of I_{Kr} can cause acquired long QT syndrome and the life-threatening ventricular tachyarrhythmia called "torsades de pointes" (Surawicz, 1989; Sanguinetti et al., 1995; Roden, 2000, 2008; Sanguinetti and Tristani-Firouzi, 2006). At the myocardial cellular level, the development of abnormal transient depolarization during AP repolarization phase called early afterdepolarization (EAD) has been considered as a trigger of lethal arrhythmias related to the usage of I_{Kr} blockers (Roden, 2000, 2008; Thomsen et al., 2003; Nattel et al., 2007; Weiss et al., 2010). Emphasis on detecting I_{Kr} blockade early in drug discovery (ICH, 2005) has contributed to the successful removal of torsades de pointes risk for new chemical entities. However, there is concern that promising new drug candidates are being unnecessarily discarded because they benignly block I_{Kr} (Sager et al., 2014; Gintant et al., 2016). Indeed, numerous examples exist of drugs that block I_{Kr} and prolong the QT interval but have little proarrhythmic risk (De Ponti et al., 2001; Redfern et al., 2003).

The human *ether-a-go-go-related gene* (hERG) encodes the ion channel through which I_{Kr} current passes (Sanguinetti et

[1]Department of Pharmacology, Graduate School of Medicine, Osaka University, Osaka, Japan; [2]Center for Advanced Medical Engineering and Informatics, Osaka University, Osaka, Japan; [3]Department of Physiology and Membrane Biology, University of California, Davis, Davis, CA; [4]Department of Physiology, Kanazawa Medical University, Ishikawa, Japan.

*K. Furutani and K. Tsumoto contributed equally to this work; Correspondence to Kazuharu Furutani: kfurutani@ucdavis.edu; Yoshihisa Kurachi: ykurachi@pharma2.med.osaka-u.ac.jp; I-S. Chen's present address is Division of Biophysics and Neurobiology, Department of Molecular and Cellular Physiology, National Institute for Physiological Sciences, Aichi, Japan.

al., 1995; Trudeau et al., 1995). We have found that some hERG blockers also increase hERG currents at potentials close to the threshold for channel activation. We refer to this electrical phenomenon as "facilitation" (Hosaka et al., 2007; Furutani et al., 2011; Yamakawa et al., 2012). A series of hERG blockers with lower proarrhythmic risk were found to evoke facilitation of hERG (Hosaka et al., 2007; Furutani et al., 2011; Yamakawa et al., 2012). The correlation between clinical safety and facilitation led to our current hypothesis: facilitation by hERG blockers increases I_{Kr} during cardiac AP repolarization and thereby decreases their proarrhythmic risk. Stringently testing this hypothesis requires a system in which facilitation can be selectively removed from an hERG blocker's mechanism. In the present study, we test the aforementioned facilitation hypothesis by developing a mathematical model of the actions of nifekalant, a hERG channel blocker that induces facilitation and has been used safely in the treatment of life-threatening ventricular tachyarrhythmias (Nakaya et al., 1993; Takenaka et al., 2001; Igawa et al., 2002; Sato et al., 2017), and calculating the impact of facilitation on the APs of human ventricular myocytes.

Materials and methods

Cell preparation and hERG channel current recording

Frogs (*Xenopus laevis*) were treated in accordance with the guidelines for the use of laboratory animals of Osaka University Graduate School of Medicine. Isolation and maintenance of the oocytes and injection with complementary RNA (cRNA) were performed as previously described (Hosaka et al., 2007; Furutani et al., 2011; Yamakawa et al., 2012). The hERG expression plasmid (provided by Drs. M.T. Keating and M.C. Sanguinetti, University of Utah, Salt Lake City, UT; Sanguinetti et al., 1995) was verified by sequencing, linearized, and transcribed in vitro using the mMESSAGE mMACHINE Transcription kit (Thermo Fisher Scientific). The oocytes were injected with 5 ng hERG cRNA and incubated at 18°C in ND96 solution (96 mM NaCl, 2 mM KCl, 1.8 mM $CaCl_2$, 1 mM $MgCl_2$, and 5 mM HEPES, pH 7.6 with NaOH) supplemented with 50 µg/ml gentamicin. Membrane currents were recorded with the two-electrode voltage-clamp technique with a GeneClamp 500 amplifier (Axon Instruments) 4–7 d after cRNA injection. The glass electrodes had resistances of 0.4–1.5 MΩ when filled with 3 M KCl. Oocytes were bathed in a low-Cl^- solution (96 mM Na-2-(*N*-morpholino) ethanesulfonic acid [NaMes], 2 mM KMes, 2 mM $CaCl_2$, 1 mM $MgCl_2$, and 5 mM HEPES, pH 7.6 with methane sulfonic acid) to minimize interference from endogenous Cl^- currents. Oocyte experiments were conducted at room temperature (22–25°C).

A human embryonic kidney (HEK) 293 cell line stably expressing hERG was provided by Dr. C.T. January (University of Wisconsin–Madison, Madison, WI) and maintained in minimum essential medium supplemented with 10% FBS and 400 µg/ml G418 (Axenia Biologix) as previously described (Zhou et al., 1998). Ventricular myocytes were enzymatically isolated from the rabbit ventricles on the day of electrophysiological experiments as previously described (Wood et al., 2018). HEK cells or cardiac myocytes used for electrophysiological study were adhered to the poly-L-lysine–coated (MW 30,000–70,000; Sigma-Aldrich; 0.1 mg/ml for 2 h at 37°C) coverslips in 12-well plates and transferred to a small recording chamber mounted on the stage of an inverted microscope (Axiovert S100; Carl Zeiss) and were continuously superfused with HEPES-buffered Tyrode's solution containing (in mM) 137 NaCl, 4 KCl, 1.8 $CaCl_2$, 1 $MgCl_2$, 10 glucose, and 10 HEPES, pH 7.4 with NaOH. Membrane currents were recorded in a whole-cell configuration established using pipette suction (Hamill et al., 1981). Leak compensation was not used. The borosilicate micropipette had a resistance of 2–4 MΩ when filled with the internal pipette solution containing (in mM) 120 KCl, 5.374 $CaCl_2$, 1.75 $MgCl_2$, 10 EGTA, and 10 HEPES, pH 7.2 with KOH. Liquid junction potential with this internal solution was less than −4 mV, and the offset was not corrected. Series resistance was typically <5 MΩ. Series resistance compensation was used when needed to constrain voltage error to <10 mV. Whole-cell recordings were performed using an Axopatch 200B patch-clamp amplifier (Molecular Devices), ITC-18 interface, and PatchMaster software (HEKA Elektronik). The data were stored on a computer hard disk and analyzed using PatchMaster and Igor Pro 7 (WaveMetrics). In AP clamp experiments, we used the human ventricular AP waveform simulated with our AP model as voltage-clamp commands. In AP recordings, ventricular myocytes were stimulated with minimal suprathreshold current pulses (2 ms) at a cycle length of 2,000 ms in whole-cell current clamp mode. Beat-to-beat instability of AP was assessed by calculating the standard deviation of APD measured at 90% repolarization, APD_{90}, based on 30 consecutive beats. EAD was defined as a transient depolarization during AP phases 2 and 3. Experiments to characterize hERG facilitation (Fig. 1; Fig. 2, A–G; Figs. S1, S2, and S3) were performed at room temperature (22–25°C), and experiments to test the prediction from simulation studies (Figs. 2 H and 11) were performed at 37.0°C, which was maintained with a CL-200A temperature controller (Warner Instruments).

Nifekalant was obtained from Nihon Schering and Cayman Chemical. Dofetilide was obtained from Alomone Labs. For comparisons of dofetilide and nifekalant effects on APs in ventricular myocyte, stock solutions were prepared, and then the researcher was blinded to their identity during experiments and analysis.

MiRP1 (KCNE2) is a β-subunit of I_{Kr} (Abbott et al., 1999). We examined whether nifekalant caused distinct effects on currents mediated by hERG alone and by hERG and KCNE2. Rat KCNE2 was provided by Dr. K. Nakajo (Jichi Medical University, Shimotsuke City, Japan), subcloned into a mammalian expression vector, pcDNA3 (Thermo Fisher Scientific), and verified by sequencing. Rat KCNE2 was cotransfected with a hERG expression plasmid and a GFP marker plasmid (pCA-GFP) into HEK293 cells by using Lipofectamine 2000 reagent (Thermo Fisher Scientific), following the manufacturer's instructions (typically 0.5 µg of total DNA/1.5 µl of Lipofectamine 2000 per well in 12-well plates). Transfected cells were identified by GFP fluorescence and modified hERG gating by KCNE (rightward shift in half-activation voltage, $V_{1/2}$; −10.4 ± 1.5 mV for hERG alone vs. −4.2 ± 2.8 mV for hERG with KCNE2; Abbott et al., 1999). We found that the drugs caused similar effects on currents from hERG + KCNE2 and hERG alone (currents not depicted) and that the $V_{1/2}$ shift due to nifekalant facilitation was similar (Table 1). As KCNE2 did not appear to impact the mechanism of facilita-

tion, we used HEK cells and oocytes expressing hERG channels alone for further experiments.

Formulations of kinetic properties for hERG current

To model the macroscopic current of hERG channels expressed in HEK293 cells, we first estimated the kinetics of the channels. The voltage-dependent activation kinetics (time constant of activation) was determined from current activation experiments (Fig. 2 A). The activation time constant was measured by fitting I_{Kr} activation at each depolarized voltage pulse, V_{depo} (typically V_{depo} greater than −40 mV), with a single exponential function:

$$I_{act}(t) = K\left[1 - \exp\left(-t/\tau_{xr}(V_{depo})\right)\right], \quad (1)$$

where K is the asymptote and $\tau_{xr}(V_{depo})$ is the activation time constant. Fig. 2 A and Fig. S3 A show the activation time constants as a function of V_{depo}. Furthermore, the voltage-dependent deactivation kinetics were divided into two processes (i.e., fast and slow processes) in accordance with the O'Hara–Rudy formalism (O'Hara et al., 2011). From current deactivation experiments (Fig. S3 B), the deactivation time constants were measured by fitting I_{Kr} deactivation at each repolarized voltage pulse, V_{repo} (typically V_{repo} less than −30 mV), to a double exponential function:

$$I_{deact}(t) = K + A_1 \cdot \exp\left[-t/\tau_{xr,fast}(V_{repo})\right] + A_2 \cdot \exp\left[-t/\tau_{xr,slow}(V_{repo})\right], \quad (2)$$

where K is the asymptote, and A_1 and A_2 are the relative components of the fast and slow processes; and $\tau_{xr,fast}$ and $\tau_{xr,slow}$ are the fast and slow deactivation time constants, respectively. Fig. S3 (C and D) shows the fast and slow deactivation time constants as a function of V_{repo}, respectively. Each time constant value in Eqs. 1 and 2 was determined by nonlinear least-squares fitting. From these experimental data and comparison with kinetics parameters of hERG channel in other experiments (Table S1), the activation and deactivation time constants were expressed as continuous functions of membrane potential, V_m, as follows (Fig. S3, E and F).

For $\tau_{xr,fast}$,

$$\tau_{xr,fast} = \frac{1{,}400}{1 + \exp\left(\frac{V_m + 10.0}{13.8}\right)} + 1{,}300 \cdot \left[\frac{1}{1 + \exp\left(-\frac{V_m + 55.0}{12.3}\right)} - 1\right]. \quad (3)$$

For $\tau_{xr,slow}$, if $V_m \geq -80$ mV,

$$\tau_{xr,slow} = \frac{5{,}000}{1 + \exp\left(\frac{V_m + 22.8}{11.5}\right)} + \frac{2{,}000}{1 + \exp\left(\frac{V_m + 25}{2.5}\right)} + \frac{4{,}000}{1 + \exp\left(-\frac{V_m + 61.5}{5.0}\right)} + \frac{3{,}000}{1 + \exp\left(-\frac{V_m + 54}{2.5}\right)} - 7{,}000, \quad (4)$$

and if $V_m < -80$ mV,

$$\tau_{xr,slow} = 2{,}000 + \frac{8{,}000}{1 + \exp\left(-\frac{V_m + 74.9}{10.2}\right)}. \quad (5)$$

Modeling of I_{Kr}

The I_{Kr} current was defined as

Table 1. **Shift of the hERG activation curve by facilitation effect**

Cells (*n*)	$\Delta V_{1/2}$ (mV)
HEK293 stably expressing hERG (7)	−26.5 ± 1.2
HEK293 transiently expressing hERG (8)	−24.9 ± 2.4
HEK293 transiently expressing hERG with KCNE2 (8)	−24.4 ± 1.1
Xenopus oocyte transiently expressing hERG (10)	−26.6 ± 1.2

$$I_{Kr} = G_{Kr} \cdot O_p \cdot R_{Kr} \cdot (V_m - E_K), \quad (6)$$

where G_{Kr} is I_{Kr} conductance (mS/μF) under the drug action, V_m is the membrane potential (mV), E_K is the reversal potential, O_p is the open state variable in the activation of I_{Kr} channel, and R_{Kr} is a time-independent function related to the inactivation property for I_{Kr}. The voltage dependence of the O_p in Eq. 6 was defined as

$$O_p = f \cdot x_{r1} + (1 - f) \cdot x_{r2}, \quad (7)$$

where x_{r1} and x_{r2} are voltage-dependent activation variables for unfacilitated and facilitated components in the I_{Kr}, respectively, and f is a fraction of unfacilitated component in I_{Kr} current. The dose–fraction relationship of f for nifekalant with an EC_{50} of 92.84 nM and a Hill coefficient (h_e) of 1.50 was represented as follows:

$$f = \frac{1}{1 + \left(\frac{[D]}{EC_{50}}\right)^{h_e}}. \quad (8)$$

In O'Hara–Rudy dynamic (ORd) model (O'Hara et al., 2011), the voltage-dependent activation variable was comprised of two variables as follows:

$$x_{ri} = A_{xr,fast} \cdot x_{ri,fast} + A_{xr,slow} \cdot x_{ri,slow}, \quad (9)$$

where i represents the voltage-dependent type, where the voltage-dependent type can be unfacilitated (x_{r1}) or facilitated (x_{r2}) activation variables, and $A_{xr,fast}$ and $A_{xr,slow}$ ($\equiv 1 - A_{xr,fast}$) are the fraction of channels with I_{Kr} activation gate undergoing fast and slow processes, respectively. The fraction $A_{xr,fast}$ was obtained as the following function that best reproduces voltage clamp experimental data (Fig. 2):

$$A_{xr,fast} = 0.05 + \frac{0.95}{1 + \exp\left(\frac{V_m + 73.4}{16.0}\right)}. \quad (10)$$

The unfacilitated (x_{r1}) and facilitated (x_{r2}) activation variables were calculated with the following first-order differential equation:

$$dx_{ri,j}/dt = \Phi \cdot \left(x_{ri,\infty} - x_{ri,j}\right)/\tau_{xr,j}, \quad (11)$$

where $x_{ri,\infty}$, for $i = 1, 2$, is the steady-state value of $x_{ri,j}$, i.e., the voltage-dependent activation curve in the hERG channel; $\tau_{xr,j}$ for j = fast, slow, is the time constant for $x_{ri,j}$; and Φ is a temperature coefficient as expressed at $3^{[(T-25)/10]}$, where T is temperature. The voltage-dependent activation curve in the hERG channel ($x_{ri,\infty}$, for $i = 1, 2$) is well represented by a single Boltzmann function. Based on our experimental data (Fig. 2, A and C), we set the Boltzmann function's half-activation voltage ($V_{1/2}$) and the slope factor to −10.7 mV and 7.4, respectively, as the voltage dependence of the unfacilitated component ($x_{r1,\infty}$) in I_{Kr} activation, and shifted the

voltage dependence of facilitated components ($x_{r2,\infty}$) in I_{Kr} activation by 26.5 mV in the negative direction (Fig. 2 G), i.e.,

$$x_{r1,\infty} = \frac{1}{1+\exp\left(-\frac{V_m+10.7}{7.4}\right)}, \quad (12)$$

$$x_{r2,\infty} = \frac{1}{1+\exp\left(-\frac{V_m+37.2}{7.7}\right)}. \quad (13)$$

Furthermore, the R_{Kr} was reconstructed as the following function that best reproduces voltage clamp experimental data (Fig. 2 A):

$$R_{Kr} = \left[0.12+\frac{0.88}{1+\exp\left(\frac{V_m+60.3}{27}\right)}\right]\cdot \left[0.32+\frac{0.68}{1+\exp\left(\frac{V_m-7}{20}\right)}\right]. \quad (14)$$

Based on our experimental measurement (Figs. 2 and S4), the G_{Kr} of when the I_{Kr} was blocked by nifekalant in a concentration-dependent manner with an IC_{50} of 145 nM and a Hill coefficient (h_i) of 1.15 was represented as follows:

$$G_{Kr} = g_{Kr}\cdot\frac{1}{1+\left(\frac{[D]}{IC_{50}}\right)^{h_i}} \quad (15)$$

where $[D]$ is the drug concentration (nM) and g_{Kr} is the I_{Kr} channel conductance absent drug. The g_{Kr} was set to 0.058 mS/μF to recapitulate the APD of endocardial myocyte represented in the ORd model (O'Hara et al., 2011).

In addition, we constructed a conventional block model modified only in I_{Kr} conductance (block without facilitation model) for comparison with the block model with facilitation.

Electrophysiological models for AP simulations

Replacing the I_{Kr} model in the original ORd model (O'Hara et al., 2011) into our aforementioned experimental based I_{Kr} model, we modified the ORd model and constructed three AP models (endocardial [ENDO], midmyocardial [MID], and epicardial [EPI]) describing cells from ENDO, MID, and EPI layers of the ventricular wall according to O'Hara et al. (2011). Scaling factors for heterogeneous model implementation are summarized in Table S2. To evaluate the impact of the I_{Kr} facilitation effect on the vulnerability for EAD development in patients with heart failure, we also constructed a heart failure model. The electrical remodeling of cardiomyocytes in failing hearts is characterized by decreases in outward ionic currents, including I_{Kr}, the slow component of the delayed-rectifier potassium current (I_{Ks}), and Na^+-K^+ pump current (I_{NaK}), as well as an increase in Na^+/Ca^{2+} exchanger current (I_{NCX}). Based on a previous study (Elshrif et al., 2015), we made several modifications of the ORd endocardial myocyte model (see details in Elshrif et al. [2015] and Table S3). These modified ORd models (non–heart failure and heart failure models) that were constructed in the present study were also implemented in an XML-based Physiological Hierarchy Markup Language (PHML), which is available as an open-access resource (http://physiodesigner.org/; Asai et al., 2013). Details on the modified ORd models as non–heart failing (and failing) endocardial myocytes with and without facilitation effect can referred from PHML models in PH database (https://phdb.unit.oist.jp/modeldb/; ID931 to 936).

For examining effects of facilitation on AP morphology, we further used two mathematical models published by ten Tusscher and colleagues (ten Tusscher et al., 2004; ten Tusscher and Panfilov, 2006; referred to as the TNNP model) representing human ventricular myocytes and by Faber and Rudy (2000) (referred to as the FRd model) representing guinea pig ventricular myocytes. The TNNP model was modified based on a previous theoretical study (Vandersickel et al., 2014) for enhancing EAD development. Furthermore, for the FRd guinea pig model, we made a few modifications based on the EPI myocyte model and constructed MID and ENDO myocyte models. Parameter modifications in both TNNP and FRd models are provided in Table S3. In both TNNP and FRd models, the facilitated component that the voltage-dependence of I_{Kr} activation shifted by 26.5 mV in the negative direction was added to each AP model.

Simulation protocol and computation

Voltage-clamping simulations for calculating I_{hERG} for each clamped voltage pulse with 4-s duration (Fig. 2) were performed using a homemade C language program, simulating by the forward Euler method with a 0.01-ms time step. The activation variables (x_{ri}, for i = 1, 2) was set equal to zero as an initial condition.

The simulated AP was calculated by the fourth-order Runge–Kutta method with double precision numbers. To minimize transient responses in each simulation, pacing stimuli of threefold diastolic threshold and the stimuli were applied repeatedly until the AP response observed in all the models reached the stationary state. To evaluate the effects of hERG channel blockade on the vulnerability of a cardiomyocyte to premature ventricular contractions, additional simulations were performed using the S1–S2 stimulation protocol: S1 stimuli until the AP converged to a steady state were applied at the stimulating frequency of 1 Hz followed by an S2 stimulus with various coupling intervals. When the effects of the hERG channel blocker on APs were examined, the stimulating frequency was set to 0.5 Hz for the ORd and TNNP models to avoid the stimulus being applied before the complete repolarization of the AP. In the FRd model, the stimulating frequency was set to 1 Hz. All simulations were encoded in C/C++ and run on an IBM-compatible computer with the Intel ICC compiler version 15.0.1. In addition, major AP simulations presented in this study can be reproduced by performing their PHML model simulations using Flint software (http://www.physiodesigner.org/simulation/flint/).

Online supplemental material

Fig. S1 shows the concentration dependence of hERG block by nifekalant and dofetilide in *Xenopus* oocytes and HEK293 cells. Fig. S2 shows the voltage dependence of induction of hERG facilitation. Fig. S3 shows the voltage dependence of activation and inactivation time constants of hERG channel. Fig. S4 shows the agreement of the concentration dependence of nifekalant-induced hERG block and facilitation in the experiments and simulations. Fig. S5 shows the impact of facilitation on the APD in normal heart. Table S1 shows the time constants of hERG/I_{Kr} ac-

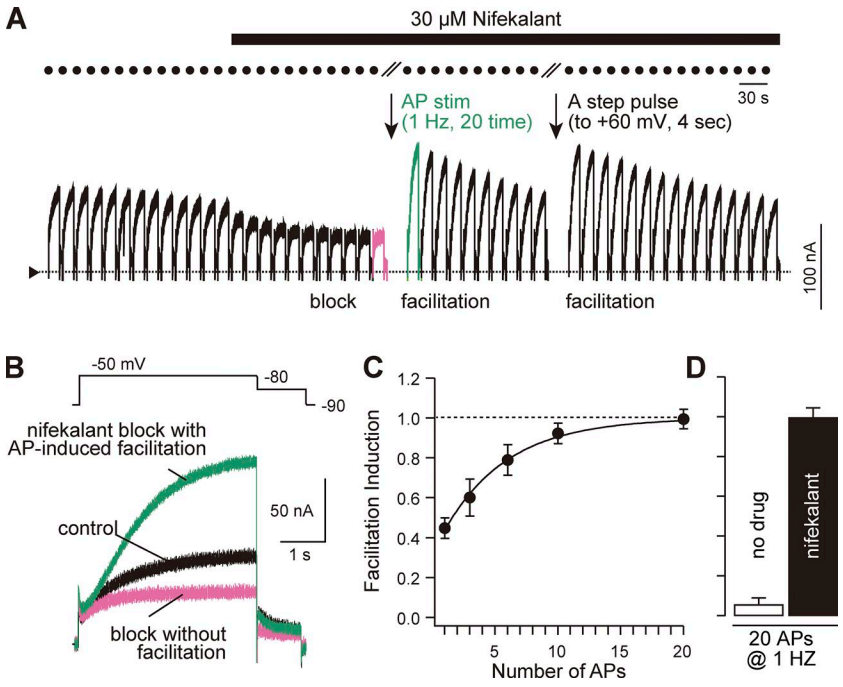

Figure 1. **Cardiac APs induce hERG facilitation with nifekalant. (A and B)** Representative cell currents from hERG channels in *Xenopus* oocytes evoked by a test pulse from holding potential of −90 to −50 mV before and after AP stimulation (1 Hz, 20×, AP waveform is the same as Fig. 2 H) and a step pulse (+60 mV for 4 s) in the presence of 30 μM nifekalant at room temperature. **(C)** AP–facilitation relation. The fraction of facilitation induced by repeating APs is normalized to the fraction induced by the +60 mV conditioning step pulse. Experimental data are means ± SEM (n = 8–15). The curve fit indicates exponential increase in the facilitation fraction by AP stimulation (facilitation = 1.02 − 0.70 · exp[−(#APs)/τ), τ = 5.45 ± 0.02]. (**D**) Requirement of nifekalant in the induction of facilitation. Effects of AP stimulation (1 Hz, 20×, AP waveform) on the increase in the hERG current were tested in the absence and presence of 30 μM nifekalant in the *Xenopus* oocytes (n = 7).

tivation and deactivation. Table S2 shows the scaling factors for heterogeneous model implementation in ORd models. Table S3 shows the modification parameters of the relevant models.

Results

AP voltage stimuli induce facilitation by nifekalant

The degree of facilitation of I_{Kr} depends on the dose of hERG blocker and the membrane's history of voltage changes. Facilitation by blockers, with the exception of amiodarone derivative KB130015 (Gessner et al., 2010), requires a preceding strong depolarization as a conditioning stimulus (Carmeliet, 1993; Jiang et al., 1999; Hosaka et al., 2007; Furutani et al., 2011; Yamakawa et al., 2012). To test whether cardiac APs are sufficient to stimulate facilitation, we applied an AP clamp protocol to hERG channels. This experiment assessed hERG current at −50 mV, a potential near its activation threshold which leaves the majority of channels closed. To achieve an adequate signal-to-noise ratio, we used *Xenopus* oocytes to express a high density of hERG channels in a membrane with minimal endogenous currents. Based on our pilot studies in *Xenopus* oocyte expression system (Figs. S1 and S2), we chose 30 μM nifekalant, the concentration close to the IC_{50} (16.6 ± 2.4 μM, n = 5), as the drug concentration to ensure that the assessment of the stimulus-dependent increases respond to preceding pulses. *Xenopus* oocytes were kept at ∼18°C until the recordings, and in our experience hERG currents, become unstable after heating to 37°C. For this reason, we recorded from oocytes at room temperature. We first confirmed that a step depolarization (+60 mV for 4 s) as a preceding conditioning pulse could induce the facilitation effect of nifekalant (Fig. 1). Similar to the strong step depolarization, repeated stimulation with a human ventricular myocyte waveform at 1 Hz induced facilitation of nifekalant-treated hERG channels (Fig. 1). The facilitation effect on hERG current saturated as the number of APs increased, indicating that facilitation reached 90% of its steady-state level within 20 heartbeats (Fig. 1 C). Without nifekalant, this voltage protocol induced little, if any, increase in hERG current (Fig. 1 D). The induction of facilitation by cardiac AP stimuli suggests that facilitation is potentially physiologically relevant.

Facilitation can be incorporated into cardiac electrophysiology modeling

To understand how facilitation could impact cellular electrophysiology mechanisms specific to human ventricular myocytes, we performed calculations with the ORd human ventricular AP model (O'Hara et al., 2011). First, we modified the I_{Kr} formula in the ORd model to reproduce hERG channel block by nifekalant, with or without facilitation. The modified I_{Kr} formula was first constrained by currents recorded from HEK cells expressing hERG (Fig. 2, A–C; and Fig. S3). These voltage clamp recordings typically required 40–60 min, and our experience conducting experiments at 37°C suggested the whole-cell recording configuration would be more stable at room temperature over these long durations. Consequently, electrophysiology on HEK cells was conducted at room temperature, and kinetics were corrected post hoc for AP modeling at 37°C. Fig. 2 shows the agreement of our I_{Kr} model with hERG current from HEK cells and its modulation by nifekalant. Left panels of Fig. 2 (D and E) show experimental hERG currents blocked with 100 nM nifekalant, before (magenta traces) and after (green traces) the induction of facilitation effect by a conditioning pulse. After the induction of the facilitation effect, nifekalant enhanced the current induced by a −30-mV pulse (Fig. 2 D), but it still suppressed the current induced by a +30-mV pulse (Fig. 2 E). The current enhancement is due to a modification of channel activation gating that shifts the voltage dependence to more hyperpolarized membrane potentials (Hosaka et al., 2007; Furutani et al., 2011). The voltage dependence of the hERG current in the facilitation condition could be

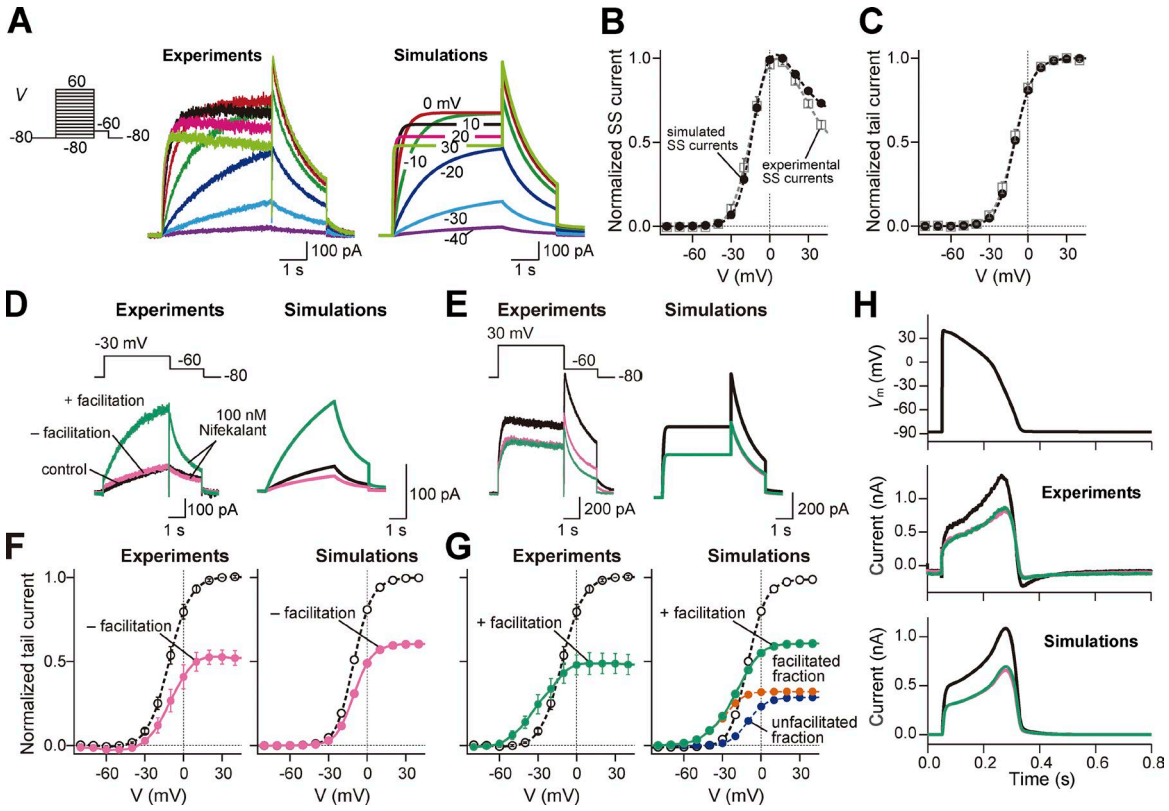

Figure 2. **Experimental and simulated macroscopic hERG/I_{Kr} currents as modified by nifekalant. (A–C)** The macroscopic hERG/I_{Kr} currents in response to voltage-clamp pulses from −80 to +60 mV in 10-mV increments from a holding potential of −80 mV at room temperature; representative traces (A), the relationship between membrane voltage and the steady-state current amplitude and membrane voltage (B), and the tail current amplitude (activation curve; C). Experimental data are means ± SEM (n = 11). **(D–G)** Simulated effects of nifekalant on hERG/I_{Kr} currents at room temperature condition. The model assumes two populations of channels, with or without facilitation effect by nifekalant (100 nM). The $V_{1/2}$ of activation for the facilitated fraction of channel was approximately −31 mV, almost 26 mV negative to that of control channel (see also Materials and methods). (D and E) The macroscopic hERG/I_{Kr} currents in response to voltage-clamp pulses from −80 to −30 mV (D) or +30 mV (E) at room temperature. (F and G) The relationship between the tail current amplitude and membrane voltage before (F) and after (G) the induction of facilitation effect. Experimental data are means ± SEM (n = 5). **(H)** The macroscopic hERG/I_{Kr} currents in response to cardiac AP at 37°C. In D–H, black, red, and green solid lines indicate with control, block with facilitation, and conventional block (block without facilitation), respectively. Under the condition in the block with facilitation, I_{Kr} comprises two fractions of I_{Kr} (see also main text), i.e., facilitated and unfacilitated fractions of I_{Kr}. In G right panel, orange and cyan dashed lines represent the facilitated and unfacilitated fractions of I_{Kr}, respectively. Experimental data are means ± SEM (n = 6–11).

described as the sum of two Boltzmann functions reflecting two populations of hERG currents having different activation voltage dependences (Furutani et al., 2011). The high-$V_{1/2}$ fraction of the channel population has biophysical characteristics typical for the hERG channel, while the low-$V_{1/2}$ fraction is facilitated. The facilitated $V_{1/2}$ was shifted negative by −26.5 mV (Table 1). This shift was consistent with that of hERG channels expressed in *Xenopus* oocytes (Furutani et al., 2011). Thus, the facilitation effect could be explained by a fraction of channels opening with a negatively shifted activation curve (Fig. 2, F and G). Inclusion of the facilitation effect in the I_{Kr} model reproduced measurements of hERG currents from voltage-step experiments (Fig. 2, D–G), and over a range of concentrations (Fig. S4). Thus, modeling facilitation as a negative shift in the voltage-dependence of a component of I_{Kr} predicted the drug-dependent facilitation of I_{Kr}.

We corrected the effect of temperature on channel gating by the equation $Q_{\Delta T} = (Q_{10})^{\Delta T/10}$, where Q_{10} is 10° temperature coefficient of 3. This method is imperfect because hERG kinetics are differentially sensitive to temperature: activation has a Q_{10} of ∼7.5, deactivation has a Q_{10} of <1.5, and inactivation and recovery from inactivation each have a Q_{10} of ∼4 (Zhou et al., 1998). However, the simple assumption of a universal Q_{10} = 3 appeared adequate: in AP clamp experiments and simulations at 37°C, our corrected I_{Kr} model predicted the effects of nifekalant on hERG currents during AP (Fig. 2 H), indicating that the model describes the block and facilitation effects of nifekalant sufficiently to allow assessment of the impact of facilitation in simulations of human ventricular myocyte electrophysiology.

Facilitation selectively increases I_{Kr} during late phase-2 and phase-3 repolarization of cardiac APs

To understand the role of facilitation in the cardiac AP, we investigated the influence of facilitation on AP morphology. When endocardial APs are evoked with 1-Hz pacing, 100 nM nifekalant prolonged the APD measured at 90% repolarization, APD_{90} (334.4 ms, vs. 257.4 ms in the control condition, see Fig. 3 A), in agreement with experimental results in human ventricular myocytes (Jost et al., 2005). The AP was slightly further prolonged in simulations with I_{Kr} block without facilitation (342.0 ms APD_{90}, compare green and magenta traces in Fig. 3 A). In

the model, 100 nM nifekalant blocks 40% of total I_{Kr} at voltages >0 mV with or without facilitation (Fig. 2 G). When facilitation is implemented in the model, 32% of the hERG channels enter a facilitated state such that they produce substantially more I_{Kr} than control conditions when the potential is between −20 and −50 mV (Fig. 2 G). There was little difference between the voltage-dependent activation variables in the I_{Kr} model during phase 1 and early phase 2 of the AP (x_{r1} and x_{r2} for the unfacilitated channels and facilitated channels, respectively), indicating that I_{Kr} behaved similarly (Fig. 3, B and C). This result is consistent with Fig. 2 H and expected, because facilitation has little impact on hERG current amplitudes at positive voltages (Fig. 2, E–G). During late phase-2 and phase-3 repolarization, an increase can be seen in I_{Kr} (asterisks in Fig. 3, A–C). However, in block conditions with or without facilitation, the APs were terminated by an increase in the inward-rectifier potassium current (I_{K1})-mediated repolarization current (Fig. 3 D) before much prolongation of the AP by facilitation. Thus, in this model of a healthy heart under unstressed conditions, only very minimal I_{Kr} facilitation is seen in simulations of facilitated I_{Kr} during late phase-2 and phase-3 repolarization of the AP (Fig. 3 B) because the facilitation effect of a negative shift in the voltage dependence of I_{Kr} activation primarily manifests in a narrow voltage range (−50 to −30 mV; see Fig. 2 G), and the AP only briefly traverses that voltage range.

Facilitation relieves reverse frequency dependence of APD prolongation

Class III antiarrhythmic agents are hERG blockers that are used clinically to suppress ventricular tachyarrhythmias (Sanguinetti and Jurkiewicz, 1990; Vaughan Williams, 1992; Sanguinetti and Tristani-Firouzi, 2006). To suppress tachyarrhythmias without provoking torsades de pointes, I_{Kr} block would ideally be use dependent and prolong APD only in response to high-frequency stimulation (Surawicz, 1989; Hondeghem and Snyders, 1990). Previous studies reported that actions of sotalol (Hafner et al., 1988; Hondeghem and Snyders, 1990) and dofetilide (Tande et al., 1990) trend against this antiarrhythmic ideal by prolonging APDs more at low than high frequencies, showing reverse frequency dependence. Notably, sotalol and dofetilide are hERG blockers that do not induce facilitation (Furutani et al., 2011; Yamakawa et al., 2012). Nifekalant also showed reverse frequency dependence, but it was not as marked (Nakaya et al., 1993; Cheng et al., 1996; Igawa et al., 2002). To determine why, we used our model to test the frequency-dependent effects of nifekalant on APD. The left panel of Fig. 4 shows changes in the APD_{90} with 100 nM nifekalant at stimulation frequencies from 0.2 to 2 Hz. Without facilitation (magenta trace in Fig. 4 A), the prolongation of APD was more effective at lower stimulation frequencies, resulting in a reverse frequency dependence. When facilitation was included in the model, the reverse frequency dependence became slightly weaker at low frequencies (green trace in Fig. 4 B). APD_{90} with facilitation was 5.5 ms shorter than without at 2.0 Hz, 7.7 ms shorter at 1.0 Hz, and 10.7 ms shorter at 0.2 Hz (Fig. 4 B). This suggests facilitation can partially relieve the reverse frequency dependence that is a risk factor for torsades de pointes.

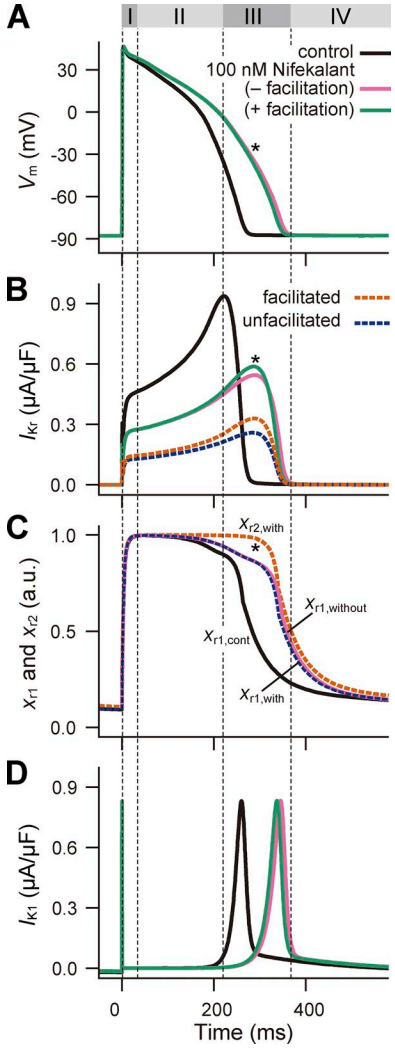

Figure 3. **Effect of I_{Kr} facilitation on cardiac AP. (A–D)** Simulated APs in an endocardial ventricular myocyte (A), I_{Kr} (B), activation state values for unfacilitated (x_{r1}) and facilitated (x_{r2}) fractions of I_{Kr} (C), and I_{K1} during APs with 100 nM nifekalant (D). Through A to D, black, green, and magenta solid lines indicate with control, block with facilitation, and conventional block (block without facilitation), respectively. In B and C, orange and cyan dashed lines represent the facilitated and unfacilitated fractions of I_{Kr}, respectively. Roman numerals above A indicate the phases of the AP in the case of with facilitation.

I_{Kr} facilitation has greater impacts on repolarization in a failing heart model

Heart failure patients are at risk for malignant ventricular arrhythmias. Clinical and theoretical data have shown that the APs in heart failure patients at slow and modest heart rates are destabilized compared with healthy subjects (Bayer et al., 2010). A more recent study indicated that the APs of the heart failure models exhibit stronger rate dependence compared with the APs of the normal model and can generate EADs and alternans at modest pacing rates (Elshrif et al., 2015). These features are thought to trigger ventricular arrhythmias (Roden, 2000, 2008; Thomsen et al., 2003; Nattel et al., 2007; Weiss et al., 2010). To determine whether facilitation might have a more critical impact on failing hearts, we investigated the frequency-dependent effects of I_{Kr} facilitation on the simulated AP in a heart failure

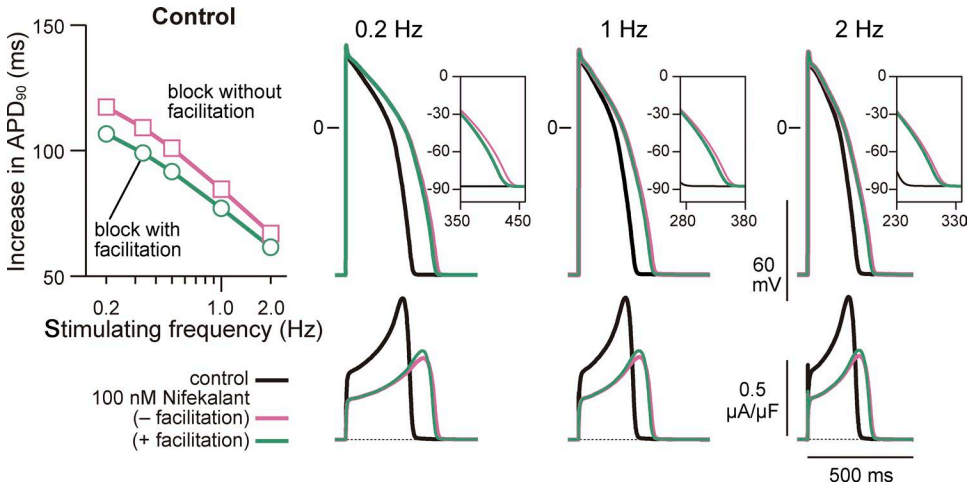

Figure 4. **Frequency-dependent effect of nifekalant on APD in non–heart failure model.** Increases in simulated APD_{90} from the control condition in normal, non–heart failure model with 100 nM nifekalant (40% I_{Kr} block) at each stimulation frequency. Effects of I_{Kr} block and facilitation on the APs in normal, non–heart failure model at various simulation frequencies with 100 nM nifekalant.

model (see Materials and methods; Fig. 5; Elshrif et al., 2015). APs in the heart failure model were prolonged from the control (non–heart failure) model (compare black traces in Fig. 4 B and Fig. 5 B) and were further prolonged by I_{Kr} blockade. The effect of facilitation was more prominent with low frequency pacing of the heart failure model, and the reverse frequency dependence of APD prolongation was more dramatically attenuated (compare Fig. 4 A and Fig. 5 A) because the delayed repolarization at low frequency pacing prolongs the latency before facilitation increases the I_{Kr} current. APD_{90} during block with facilitation was 16.5 ms shorter than without facilitation at 2.0 Hz, 36.3 ms shorter at 1.0 Hz, and 53.0 ms shorter at 0.2 Hz (Fig. 5 B), suggesting that the electrical remodeling in failing myocytes makes cellular responses more sensitive to I_{Kr} modulation.

I_{Kr} facilitation prevents EAD

Excessive AP prolongation by a hERG blocker showing strong reverse frequency dependence creates an electrophysiological

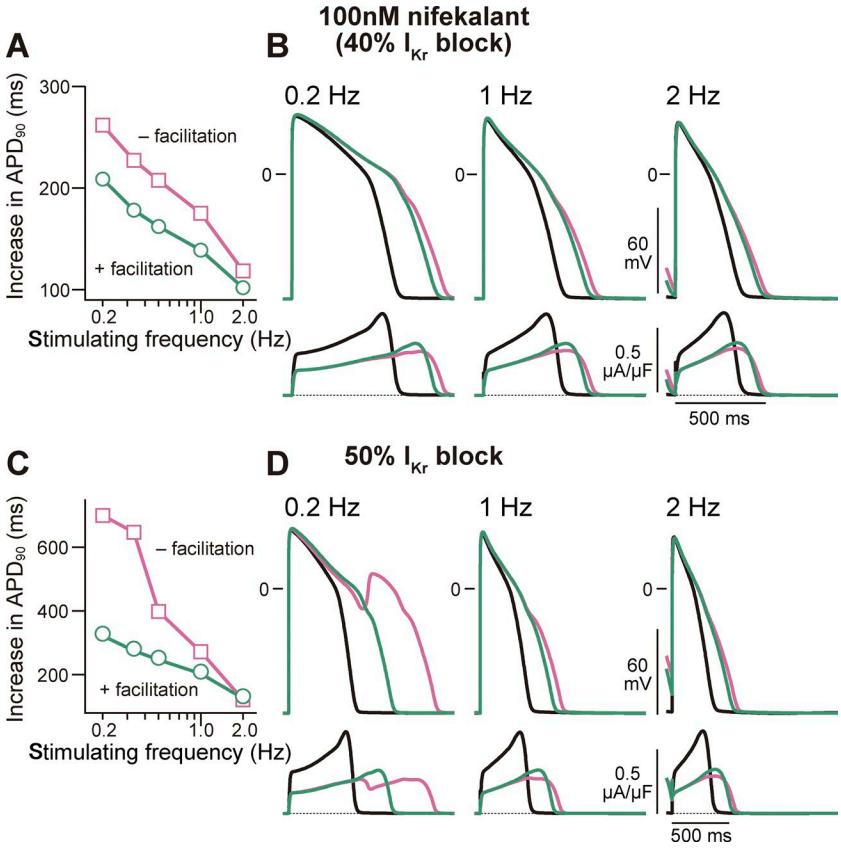

Figure 5. **Frequency-dependent effect of nifekalant on APD in heart failure model. (A and C)** Increases in simulated APD_{90} from the control condition in heart failure model with 100 nM nifekalant (40% I_{Kr} block; A) and 50% I_{Kr} block (C) at each stimulation frequency. **(B and D)** Effects of I_{Kr} block and facilitation on the APs in heart failure model at various simulation frequencies with 100 nM nifekalant (40% I_{Kr} block; B) and 50% I_{Kr} block (D). The small "hook" at the beginning of the AP of 2 Hz is the repolarization phase of the previous one.

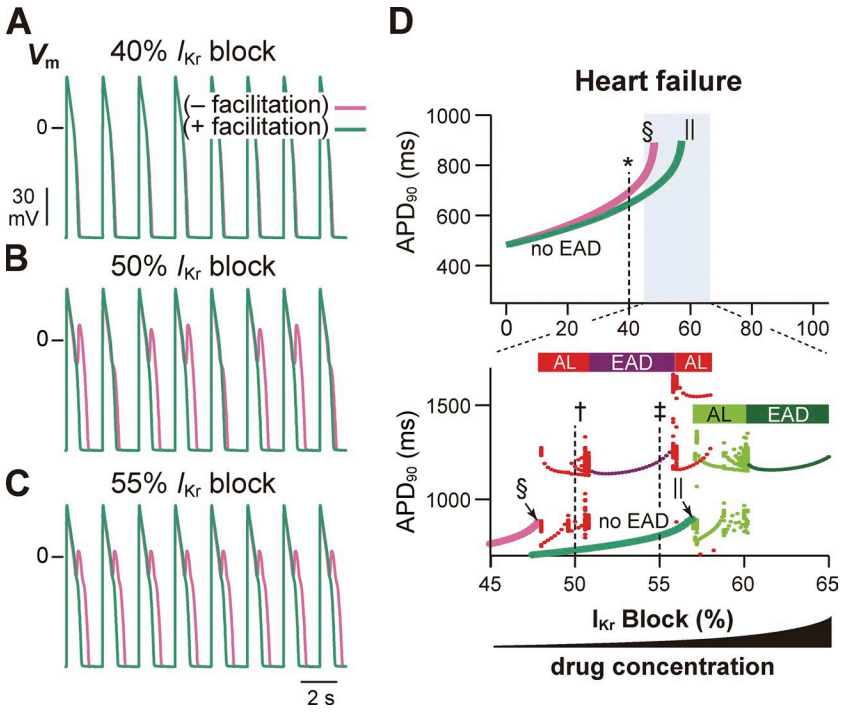

Figure 6. **The effect of I_{Kr} facilitation on the APD prolongation and EAD development by I_{Kr} block. (A–C)** The steady-state AP trains with 40% (A), 50% (B), and 55% (C) I_{Kr} block in heart failure model with and without facilitation. **(D)** Effect of I_{Kr} block and facilitation on the APD and the development of EADs in heart failure model. Green and magenta lines indicate APD_{90} of AP (without EAD) for block with facilitation or block without facilitation, respectively. Asterisk, dagger, and double dagger indicate the conditions in A–C, respectively. Sections and pipes indicate the upper limits of I_{Kr} block where APs were normally terminated. When EAD was observed, it was classified as either alternated EAD or periodic EAD. In the bottom panel of D, red and deep purple dots indicate APD_{90} of AP with EAD for block without facilitation, while light and deep green dots indicate APD_{90} of AP with EAD for block with facilitation. Horizontal bars above the dots indicate alternated EAD, AL, or periodic EAD, EAD; see also main text.

environment that favors the development of EAD at low stimulating frequencies. Increasing I_{Kr} block from 40% to 50% caused further APD prolongation (Fig. 5, C and D). Without facilitation, the APD was dramatically prolonged with low-frequency pacing (magenta trace in Fig. 5 C). We found that in the heart failure model paced at 0.2 Hz, EAD appeared at 50% I_{Kr} block without facilitation (magenta traces in Fig. 5 D), and facilitation suppressed these EADs (green traces in Fig. 5 D). Although this pacing is unphysiologically slow, these findings suggest hERG facilitation could have a more significant impact on arrhythmogenesis in a failing heart.

To determine the range of conditions over which facilitation could potentially suppress proarrhythmic effects of hERG blockade, we extended analysis in the heart failure model. Fig. 6 (A–C) shows examples of steady-state AP trains in several I_{Kr} block conditions. Fig. 6 D shows the changes in APD_{90} as a function of the degree of I_{Kr} block. Below 40% block, the drug prolonged APD_{90} similarly with or without facilitation (Fig. 6, A and D). Without facilitation, APs were destabilized when I_{Kr} inhibition was >48% (§ in Fig. 6 D; APD_{90} = 890.0 ms), resulting in alternating EADs and periodic EADs. In the bottom panel of Fig. 6 D, we plot APD_{90} of AP with EAD; alternating EADs (AL, red), and periodic EADs (EAD, deep purple) occur at distinct degrees of I_{Kr} block. With facilitation, EADs did not appear until 57% inhibition of I_{Kr} (|| in Fig. 6 D; APD_{90} = 896.4 ms), indicating that I_{Kr} facilitation stabilized the AP. Fig. 6 (B and C) shows examples of steady-state AP trains with 50% and 55% block of I_{Kr} (conditions indicated by † and ‡ in Fig. 6 D, bottom), respectively. These results suggest that the facilitation of I_{Kr} by blockers reduces proarrhythmic side effects by preventing the development of EADs. In the non–heart failure model of an endocardial cell, a similar antiarrhythmic effect of facilitation was observed with more extreme I_{Kr} blockade (Fig. 7 top left and Fig. S5).

APs are heterogeneous between different regions of the ventricles (Drouin et al., 1995,; Konarzewska et al., 1995; Näbauer et al., 1996; Szabó et al., 2005). To test whether the facilitation effects are generalizable to models of myocardial cells from other layers of the ventricular wall or just an oddity of one model of an endocardial cell, we similarly constructed two other AP models (MID, EPI) describing cells from midmyocardial and epicardial layers (O'Hara et al., 2011). We found that I_{Kr} facilitation can prevent EAD development not only in the endocardial cell but also in the MID and EPI models (Fig. 7). In addition to the ORd models, we tested if I_{Kr} facilitation prevents EAD development in the TNNP human ventricular AP models (ten Tusscher et al., 2004; ten Tusscher and Panfilov, 2006) and in the FRd guinea pig ventricular AP model (Faber and Rudy, 2000). These models differ in the AP configuration/duration and the vulnerability of the regular AP termination to the decrease in I_{Kr}. Kinetic parameters of the I_{Kr} formula of TNNP models and FRd models are different from those of our modified ORd models. The differences in the ventricular AP models affect the impact of I_{Kr} facilitation on AP, but I_{Kr} facilitation has a similar preventive effect on EAD development in each model (Fig. 7). This suggests that prevention of EAD development is not an oddity exclusive to any one model and may be a general cardiac electrical phenomenon resulting from facilitation of I_{Kr} by blockers. Next, we studied the ionic mechanism by which I_{Kr} facilitation prevents EAD development in a cardiac myocyte model.

I_{Kr} facilitation suppresses reactivation of L-type Ca^{2+} channels. In the heart failure model at 55% inhibition of I_{Kr} without facilitation (magenta lines in Fig. 8, left), the repolarization delay caused by I_{Kr} reduction augmented the window current in L-type Ca^{2+} channel current (I_{CaL}) during late AP phase 2 with each stimulation (Fig. 8 C, left). As a result, the evoked APs were gradually prolonged with each stimulation, leading to further augmenta-

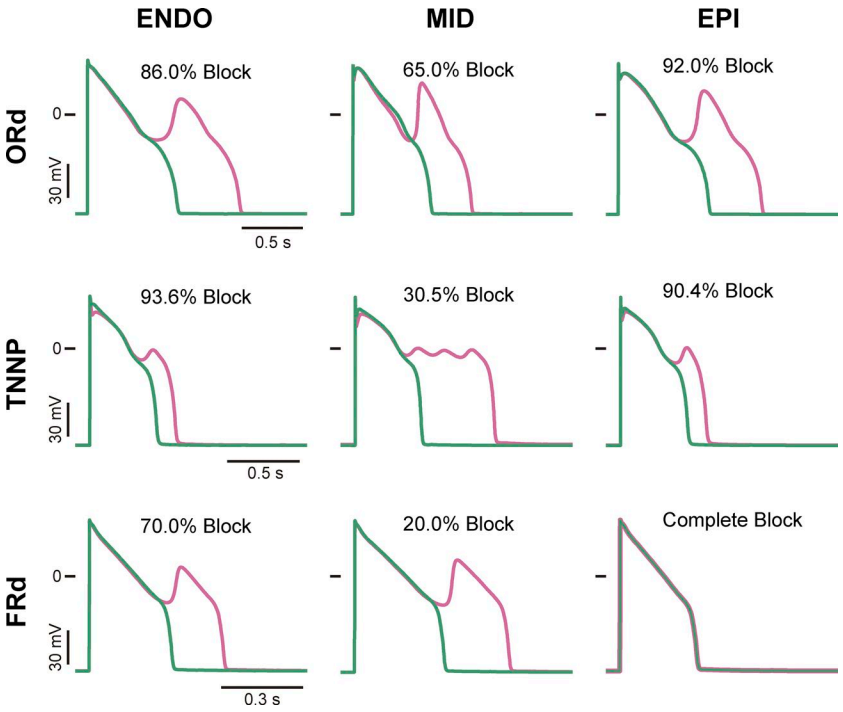

Figure 7. **The preventive effects of I_{Kr} facilitation on EAD development in several ventricular AP models.** Simulated AP responses in the modified ORd human ventricular myocyte AP models, the modified TNNP human ventricular myocyte AP models, and the modified FRd guinea pig ventricular myocyte AP models of ENDO, MID, and EPI cells. APs in ORd and TNNP models were stimulated at 0.5 Hz, while APs in FRd model were stimulated at 1 Hz. In each panel, the intensity of I_{Kr} block is indicated as % Block. Magenta lines indicate AP responses in the I_{Kr} block without facilitation, while green lines indicate AP responses in the I_{Kr} block with facilitation at the same degree of I_{Kr} block as the overlaid magenta line (as an exception, in FRd model of EPI cell, EAD was not observed even by complete I_{Kr} block).

tion of the I_{CaL} window current (Fig. 8 C, left) and AP prolongation (Fig. 8 B, left). Then, the stagnated repolarization caused more reactivation of L-type Ca^{2+} channels (arrowhead in Fig. 8 C, left), enhancing an inward current component of the net ionic current (I_{net}) during late AP phase 2 (Fig. 8 D, left). This caused the inward-outward balance of I_{net} (asterisks in Fig. 8 D, left) that temporally interrupted AP repolarization, followed by a second rising phase of the AP that led to EAD. This I_{Kr} block-induced dysfunction eventually converged to a periodic EAD response (Fig. 6 C; Fig. 8 A, right column). In contrast, an increase in I_{Kr} due to facilitation (blue arrow in Fig. 8 E, right) enhanced an outward current component in I_{net} during late AP phase 2 and phase 3 (Fig. 8 D, right). This accelerated the membrane repolarization and completed the AP repolarization (Fig. 8 B, right). Thus, facilitation suppresses EADs by selectively amplifying I_{Kr} during late phase 2 and phase 3 of APs when the repolarization is in danger of stagnating. The facilitated I_{Kr} overwhelms the reactivating I_{CaL}, preventing EAD.

Modeling suggests that I_{Kr} facilitation could improve patient safety

Class III antiarrhythmic agents are powerful antiarrhythmics used to treat patients with serious ventricular tachycardias in spite of their narrow therapeutic index (Tamargo et al., 2015). The maximal therapeutic dose of class III antiarrhythmics is generally limited by proarrhythmic risk of I_{Kr} block. At low doses with minimal proarrhythmic risk, nifekalant suppresses malignant ventricular tachyarrhythmia (Takenaka et al., 2001) and improves short-term and long-term survival of adult patients with ventricular fibrillation/pulseless ventricular tachycardia (Sato et al., 2017). In animal models, a torsades de pointes response was not detected with the therapeutic dose of nifekalant (Satoh et al., 2004), and nifekalant has a broader safety window than I_{Kr} blockers without facilitation (Sugiyama, 2008; Yamakawa et al., 2012). To determine whether nifekalant's favorable safety profile could be related to the facilitation mechanism, we conducted simulations of nifekalant's predicted safety window with and without facilitation.

We calculated the "therapeutic" dose of nifekalant that prolongs APD_{90} by 500 ms, an established clinical standard (Igawa et al., 2002; Drew et al., 2010). With facilitation, the simulated therapeutic dose was 278.9 nM (68.0% I_{Kr} block); without facilitation, 14% less drug was required, 240.2 nM (64.1% I_{Kr} block; Fig. 9). To confirm the antiarrhythmic effect of nifekalant at those therapeutic doses, we assessed the vulnerability of cardiomyocytes to premature excitation. We measured the refractory period of APs in the normal, non–heart failure model by calculating the shortest timing sufficient to produce secondary voltage overshoot by a second stimuli (S2 stimuli) after regular pacing (S1-S2 stimulation protocol). The effective refractory periods with nifekalant were 216 or 215 ms longer than control, with or without facilitation, respectively (Fig. 9), suggesting that facilitation has little impact on effectiveness as a class III antiarrhythmic. We simulated the safety window for nifekalant as the ratio of the dose that produces toxicity (EAD) to the therapeutic dose. Without facilitation, EADs occurred at 657.5 nM, 2.74× the calculated therapeutic dose (Fig. 10). With facilitation, EADs did not occur until 894.5 nM, 3.21× the therapeutic dose. Thus, facilitation widens the simulated safety window for EADs, suggesting that with facilitation an I_{Kr} blocker can remain an efficacious class III antiarrhythmic agent, with an improved safety profile.

Finally, we empirically tested the prediction that nifekalant is less likely to induce EAD than a hERG blocker without facilitation effect. Like nifekalant, dofetilide is a hERG channel blocker developed as a class III antiarrhythmic agent, but it carries significant torsades de pointes arrhythmia risk (Jaiswal and Goldbarg,

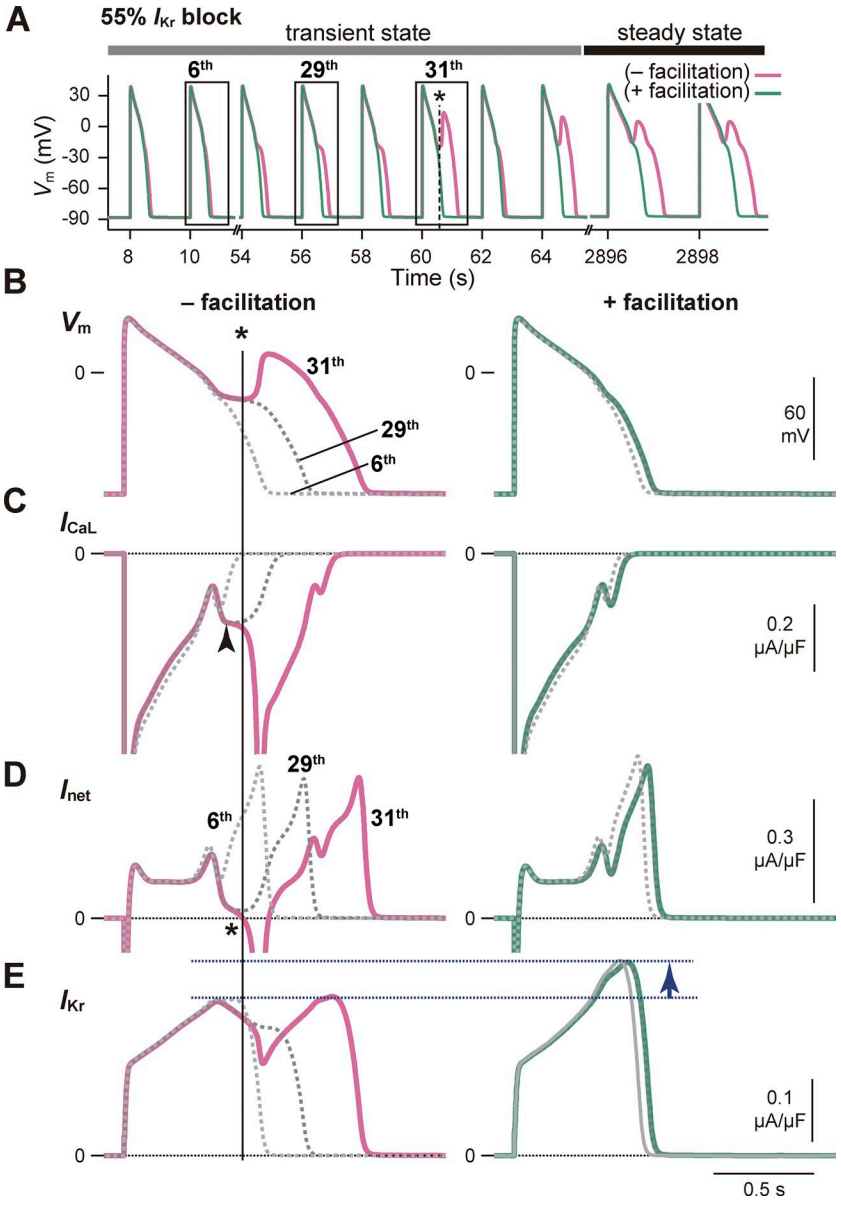

Figure 8. **Ionic mechanism of EAD development by I_{Kr} block and the influence of I_{Kr} facilitation. (A–E)** Simulated APs and the changes in the membrane potential (V_m; A and B), L-type Ca^{2+} channels current, I_{CaL} (C), the net ionic current, I_{net} (D), and I_{Kr} (E) during APs with 55% I_{Kr} block in heart failure model. Each simulation of block (left) and facilitation (right) was started from the same initial values. In each panel of B–E, three curves are overlaid. Thin dashed line, thick dashed line, and solid line indicate 6th, 29th, and 31st AP responses after the 55% I_{Kr} block, respectively, and these APs are marked with squares in A. In C, an arrowhead indicates the time point of the reactivation of L-type Ca^{2+} channels, and asterisks indicate the time point of the inward-outward balance of I_{net} in 31st AP response in the case without facilitation (magenta solid line; see also main text). In E, the increase in the I_{Kr} current in the case with facilitation is highlighted by two horizontal dashed lines and an arrow.

2014), especially in patients with congestive heart failure (Torp-Pedersen et al., 1999; Brendorp et al., 2002). Unlike nifekalant, dofetilide does not cause facilitation of hERG channels (Furutani et al., 2011). The cellular mechanisms of EADs upon I_{Kr} block have been extensively studied in isolated rabbit ventricular myocytes (Zhou et al., 1995; Studenik et al., 2001; Xu et al., 2001; Choi et al., 2002; Aiba et al., 2005; Xie et al., 2009; Sato et al., 2010; Maruyama et al., 2011; Zhao et al., 2012), and we chose this well-characterized preparation to compare EAD induction by nifekalant and dofetilide. We first determined if EADs could be induced by dofetilide block. Previous reports indicated that 1 μM dofetilide, but not 100 nM, can induce EADs in isolated rabbit ventricular myocytes (Xu et al., 2001; Nalos et al., 2012). Consistent with these previous findings, we observed EADs after application of 1 μM dofetilide in isolated rabbit ventricular myocytes AP stimulated at 0.5 Hz at 37°C. We then determined the dose of nifekalant expected to produce a similar degree of I_{Kr} block. In hERG channels expressed in HEK293 cells and voltage clamped at room temperature, the IC_{50} for nifekalant block (142.6 ± 13.1 nM, n = 6) was 5.1× higher than that for dofetilide block (27.7 ± 5.5 nM, n = 6; Fig. S1). For experiments in myocytes, we compared a 10× higher dose, 10 μM nifekalant versus 1 μM dofetilide, to ensure that nifekalant blocked I_{Kr} more than dofetilide. In experiments where the researcher was blinded as to whether dofetilide or nifekalant were applied, we found that 1 μM dofetilide induced alternant EADs in 26% (5 of 19 myocytes) of rabbit ventricular myocytes, but 10 μM nifekalant did not induce EADs (0 of 19 myocytes; Fig. 11, A and B). When the data from the five dofetilide-treated myocytes showing APs with EADs were excluded from the analysis, the mean APD_{90} with 10 μM nifekalant was 11.5 ms shorter than those with 1 μM dofetilide (Fig. 11, C and D). This indicates that dofetilide has a more extreme broadening effect on APs than nifekalant, even when EAD does not occur. The beat-to-beat instability, which is another indicator of AP destabilization, was similar between nifekalant and dofetilide groups (dofetilide APD_{90} std = 25.6, nifekalant APD_{90} std = 23.1). These

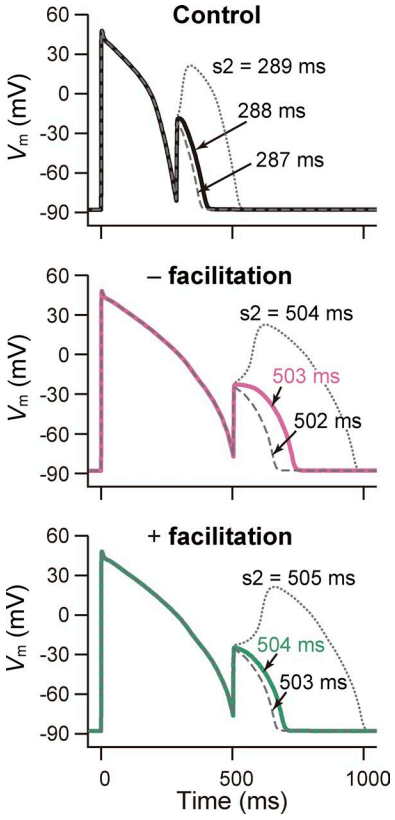

Figure 9. **The antiarrhythmic effect of I_{Kr} facilitation.** Simulation of block and facilitation effect on the reexcitation by the second stimulation (S2) in the ORd model of nonfailing ENDO cell with the prolonged APD_{90} by 500 ms. AP responses to the S2 stimuli applied at the time indicated.

findings are consistent with our conclusion that facilitation of hERG channels suppresses the EAD developments in ventricular myocytes, as predicted by simulation studies.

Discussion

The objective of this study was to examine the influence of the facilitation mechanism on electrical activity in cardiomyocytes. This mathematical model represents a general view of the role that facilitation may play with I_{Kr} blockers. We found that I_{Kr} facilitation effects on simulated cardiac APs depended on the AP morphology and APD. Facilitation enhances I_{Kr} during prolonged APs. The repolarizing effect of facilitated I_{Kr} is augmented at low frequencies and as APD prolongs, thus avoiding repolarization reserve impairment and suppressing EAD development. Therefore, hERG channel blockers with facilitation may offer a safety advantage for arrhythmia treatment.

In a previous article (Furutani et al., 2011), we proposed that the increase in hERG current by facilitation could result from blockers binding to a second site on the channel. In this "two-site" model, increased current arises from a population of channels with blocker bound to a facilitation site causing a shift of voltage-dependent activation gating to more negative potentials. Herein, we used an analytic Hodgkin–Huxley formulation of the two-site model to recapitulate nifekalant's actions on I_{Kr} current as the sum of facilitated and unfacilitated fractions (see Materials and methods). This empirical kinetic description enabled practical calculations of macroscopic electrical responses (Fig. 2), to model how facilitation could impact cellular electrophysiology mechanisms specific to human ventricular myocytes.

We do not yet understand how nifekalant increases the activity of hERG channels in terms of statistical thermodynamics. Facilitation and blockade appear to be inextricably intertwined, as all drugs that cause hERG facilitation are pore blockers of the channel (Carmeliet, 1993; Jiang et al., 1999; Hosaka et al., 2007; Gessner et al., 2010; Furutani et al., 2011; Yamakawa et al., 2012). However, certain mutations in hERG's S6 helix that lines the K^+ conduction path affect facilitation without affecting block, suggesting that drug–channel interactions within the pore are involved in facilitation (Hosaka et al., 2007). This suggests that the coupling between block and facilitation can be altered. Another important characteristic of hERG facilitation is that it requires a preceding depolarization. The voltage dependence of the development of facilitation in the presence of nifekalant was fitted by single Boltzmann function with $V_{1/2}$ of –19.3 ± 0.9 mV and k of 7.4 ± 0.8 (Fig. S2). Such voltage dependence is similar to the voltage dependence of hERG activation (Table 1, in *Xenopus* oocytes at room temperature), suggesting the hERG channel opening has a role in developing facilitation effect. In the future, we hope to develop a more satisfying Markov-chain type model based on Eyring rate theory that captures the microscopic kinetics of binding and conformational changes that underlie nifekalant's actions.

Our conclusions are based on modeling, yet suggest a general cardioprotective mechanism. To exert cardioprotective effects in vivo, certain conditions are required. First, the concentration of the hERG blocker needs to be in a range conducive to facilitation. Second, the membrane potential must depolarize sufficiently to induce the I_{Kr} facilitation effect. We have previously reported the concentration- and voltage-dependence relationships be-

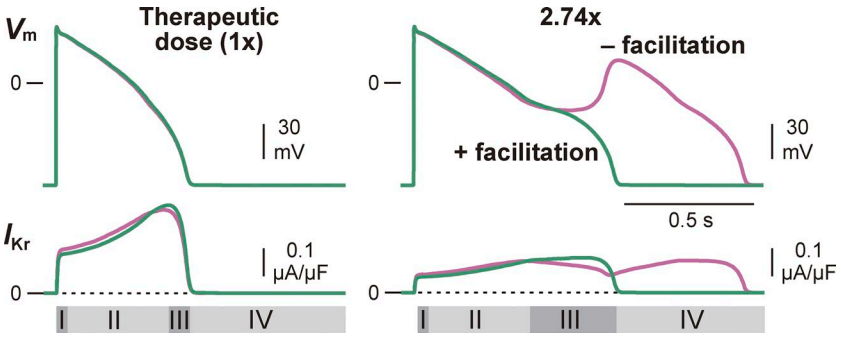

Figure 10. **Effect of I_{Kr} facilitation on the safety window of nifekalant.** The changes in the membrane potential (V_m; upper) and I_{Kr} (lower) in the presence of various concentrations of nifekalant in normal, non–heart failure model. The therapeutic dose is set as the concentration that prolongs APD_{90} by 500 ms and effectively suppresses the ectopic excitation as shown in Fig. 9. 2.74× indicates 2.74 times higher drug concentration compared with its therapeutic dose (1×). Green and magenta lines indicate I_{Kr} block with and without facilitation, respectively. Roman numerals at the bottom indicate the phases of the AP with facilitation.

tween block and facilitation for several drugs in hERG channels expressed in *Xenopus* oocytes (Furutani et al., 2011; Yamakawa et al., 2012). In the present study, we evaluated the concentration dependence of nifekalant on hERG channels expressed in HEK293 cells (Fig. S1 and Table 2). As in oocytes, the IC_{50}/EC_{50} for block and facilitation by nifekalant were similar (92.84 ± 7.71 nM for facilitation; 142.6 ± 13.1 nM for block; Table 2). However, for other class III antiarrhythmic agents, the concentration dependences of block and facilitation are distinct. For example, the EC_{50} for I_{Kr} facilitation by amiodarone is lower than that for IC_{50} block (Furutani et al., 2011). These data indicate that when these agents are administered in the treatment of arrhythmias at concentrations effective for block, they certainly also reach the effective concentration for facilitation. Our experimental data show that facilitation by nifekalant could be induced by cardiac APs (Fig. 1). An important finding of this work is that facilitation had a negligible impact on APs under normal conditions (Fig. 3 and Fig. 4), suggesting that facilitation would not greatly affect normal ECGs. Our simulation study suggests that facilitation may have a selective impact during severe repolarization impairment and heart failure conditions, leading to a lower risk of arrhythmias.

Table 2. **Effects of nifekalant on hERG channels: Dose–response (*n* = 9)**

Drug effect	IC_{50}/EC_{50} (nM)	Hill coefficient
Block	142.6 ± 13.1	1.10
Facilitation	92.8 ± 7.7	1.50

It is widely accepted that I_{Kr} plays an important role in the repolarization of the AP (Surawicz, 1989; Sanguinetti and Jurkiewicz, 1990; Zeng et al., 1995; Clancy et al., 2003; Sanguinetti

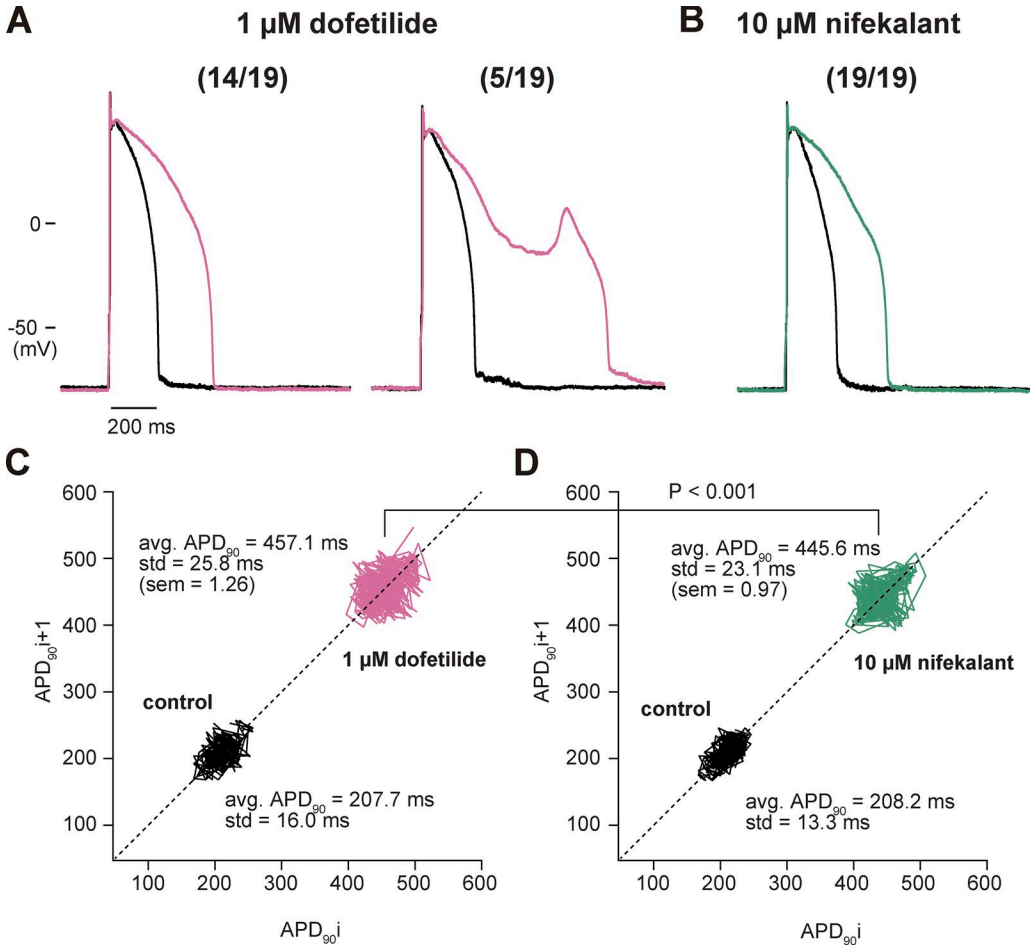

Figure 11. **Rabbit cardiac myocyte APs are more stable in nifekalant than dofetilide.** AP responses in the isolated rabbit ventricular myocytes were stimulated by minimal current injection at 0.5 Hz in whole-cell current clamp mode at 37°C. **(A and B)** After recording of the control responses (black lines), cells were treated with either 1 μM dofetilide (pink lines) or 10 μM nifekalant (green line). (A) Representative AP responses without (left) or with (right) EAD in 1 μM dofetilide. Of 19 cells treated with 1 μM dofetilide, five cells showed EAD responses (26%). 14 cells showed the prolongation of APD in 1 μM dofetilide but did not show EAD responses. (B) Representative AP responses in 10 μM nifekalant. All cells treated with 10 μM nifekalant showed prolongation of APD upon 1 μM dofetilide but did not show EAD responses. **(C and D)** Prolongation of APD and beat-to-beat instability by 1 μM dofetilide and 10 μM nifekalant. Only the data from the cells showing AP responses without EAD were included in this analysis (14 cells of 1 μM dofetilide-treated group; 19 cells of 10 μM nifekalant-treated group). 30 consecutive APs responses in control and under the treatment of either 1 μM dofetilide or 10 μM nifekalant were recorded, and APD_{90} of the *i*+1th action potential ($APD_{90}i+1$) was plotted against APD_{90} of the one action potential before (*i*th; $APD_{90}i$). APD_{90}s were prolonged by treatment with 1 μM dofetilide (C) or 10 μM nifekalant (D) compared with control. 1 μM dofetilide prolonged APD_{90} longer ($P = 4.26 \times 10^{-13}$, Student's *t* test) than 10 μM nifekalant. The control APD_{90}s were identical between dofetilide- and nifekalant-treated cells (P = 0.58).

and Tristani-Firouzi, 2006). The decrease in I_{Kr} is believed to be associated with EADs, an important cause of lethal ventricular arrhythmias in long QT syndrome and heart failure. Experiments by Guo et al. (2011) in isolated nonfailing human endocardial ventricular myocytes showed EADs in the presence of the I_{Kr} blocker dofetilide (0.1 µM, corresponding to ∼85% I_{Kr} block; Thomsen et al., 2003), which induces torsades de pointes arrhythmias (Thomsen et al., 2003). In the present study using the modified ORd model, we successfully reproduced the experimental results of Guo et al. (2011), as did the original ORd model (O'Hara et al., 2011). In rabbit ventricular myocytes, we observed EADs with low incidence (26%) in the presence of 1 µM dofetilide. Our result is qualitatively consistent with a previous study that found 1 µM dofetilide induced EADs in a subset (65%) of rabbit ventricular myocytes (Nalos et al., 2012). 10 µM nifekalant did not induce EAD under these same conditions, consistent with models predicting that facilitation prevents EADs. In HEK293 cells either 1 µM dofetilide or 10 µM nifekalant blocks >99% of hERG current (Figs. 11 and S1), which suggests only a small fraction of I_{Kr} might be available to be facilitated. However, these hERG blockers act by partitioning into the cell membrane to access cells, and can have dramatically different IC_{50} values in different cell types (e.g., IC_{50} for HEK293 cell vs. *Xenopus* oocytes were 142.6 ± 13.1 vs. 16.6 ± 2.4 µM for nifekalant, respectively; 27.7 ± 5.5 vs. 441.6 ± 24.8 nM for dofetilide, respectively; Fig. S1 and Furutani et al., 2011). hERG blockers have been found to be less effective inhibitors of I_{Kr} from isolated myocytes than hERG block in HEK293 cells. For example, E-4031 blocks hERG current in HEK293 cells with an IC_{50} of 7.7 nM (Zhou et al., 1998) and blocks I_{Kr} from rabbit ventricular myocytes with an IC_{50} of ∼20 nM (Zhou et al., 1995, 1998).

Reverse frequency–dependent action on APs is a property common to class III antiarrhythmic agents (Hafner et al., 1988; Hondeghem and Snyders, 1990; Tande et al., 1990; Carmeliet, 1993; Jurkiewicz and Sanguinetti, 1993; Nakaya et al., 1993; Jiang et al., 1999), and the associated proarrhythmic risk limits their clinical usefulness (Hondeghem and Snyders, 1990; Okada et al., 1996). Reverse frequency dependence of I_{Kr} block was first explained by an increase in the slowly activated delayed-rectifier K^+ current with rapid heart rates (Jurkiewicz and Sanguinetti, 1993). Drug mechanisms can prolong APD at higher stimulation frequencies to attenuate reverse frequency dependence (Hondeghem and Snyders, 1990). For example, some I_{Kr} blockers, such as vesnarinone, have high affinities to opened and/or inactivated hERG channels and exhibit an accumulation of inhibition at higher stimulation frequencies (use-dependent block), reducing proarrhythmic risk (Toyama et al., 1997). In our model, I_{Kr} block is not altered by stimulation frequency. Therefore, the reverse frequency dependence may be even less than predicted. Facilitation attenuates reverse frequency dependence by enhancing I_{Kr} during late phase 2 and phase 3. The effect on reverse frequency dependence becomes more prominent at higher concentrations of drug. Fig. 4 and Fig. 5 (A and B) show the effects of the modest I_{Kr} block by 100 nM nifekalant (∼40% I_{Kr} block and ∼32% I_{Kr} facilitation). When the drug concentration increased, the effect of facilitation was more prominent (Fig. 5, C and D) because of the concentration-dependent increase in the facilitated fraction and the prolonged phase 2–3 of AP. Under the higher concentrations of blocker, EADs and alternans emerged at low frequencies that dramatically affect APD (Fig. 5, C and D). These EADs were effectively suppressed by I_{Kr} facilitation (Figs. 6, 7, 8, and S5).

Previous studies showed that I_{CaL} reactivation is crucial for the development of EADs (Zeng and Rudy, 1995; O'Hara et al., 2011; Tsumoto et al., 2017). Prolongation of the time at plateau voltages caused by I_{Kr} block allows I_{CaL} reactivation (O'Hara et al., 2011). The EAD initiation mechanism in the present study is consistent with an I_{CaL} reactivation mechanism (Fig. 8). I_{Kr} facilitation accelerates the repolarization just before I_{CaL} reactivation (Fig. 8). Therefore, the inward-outward balance of I_{net} during the plateau and AP phase 3 is one determinant for the development of EADs. Such inward-outward balance of I_{net} results from the interaction of ionic mechanisms underlying the cardiac AP. In addition to an increase in I_{Kr} by facilitation, these secondary changes may contribute to preventing I_{CaL} reactivation and development of EADs.

Our modeling and experiments indicate that I_{Kr} facilitation prevents EAD development, which may decrease proarrhythmic risk. In considering the clinical and physiological relevance of facilitation to class III antiarrhythmic agents, it is important to be aware of the limitations of our study. The models only approximate currents from isolated myocytes. The absolute voltage and concentration dependence of facilitation has not yet been determined with native I_{Kr} currents at physiological temperature. Our model of I_{Kr} facilitation was constrained by hERG currents from HEK cells recorded at room temperature, and the effect of temperature was imperfectly corrected. We have not yet examined the facilitation effect on native tissues. Additionally, off-target effects of blocker may cause further changes, although appreciable cardiac off-target effects of nifekalant have not yet been found. The experiments conducted with rabbit myocytes here are limited, and are just the beginnings of an in-depth study into induction of EADs by drugs with and without facilitation. These types of experiments serve as an important empirical test of our hypothesis, but ultimately will lack the precision of modeling results, as we are unlikely to find hERG blockers with and without facilitation that otherwise have identical binding and dissociation properties. Therefore, a combination of cardiac AP modeling and experiment are expected to provide greater insights than either alone.

These limitations notwithstanding, this study sheds light on the potential impact of facilitation on cardiac safety. As EAD is considered to be a trigger of drug-induced ventricular tachycardia and torsades de pointes arrhythmia (Roden, 2000, 2008; Thomsen et al., 2003; Nattel et al., 2007; Weiss et al., 2010), facilitation defines a novel mechanism that could suppress proarrhythmic risk and broaden the safety window of hERG blocking agents. The facilitation effect may explain the reason many clinically useful drugs, especially class III antiarrhythmic agents, are surprisingly safe, despite hERG block and QT interval prolongation. Meanwhile, a lack of a facilitation effect may explain why dofetilide, d-sotalol, atenolol, and terfenadine have a high risk for lethal arrhythmia (Furutani et al., 2011; Yamakawa et al., 2012). Recent studies have described the general utility of the in silico integration of drug effects on multiple cardiac currents to reduce false-positive and false-negative classifications based on hERG block alone (Mirams et al., 2011; Kramer et al., 2013). More elab-

orate models incorporating detailed descriptions of ion channel modulation and experimental tests will improve future investigations of the mechanisms underlying the proarrhythmic risk of class III antiarrhythmic agents.

In conclusion, we propose that hERG blockers with facilitation effects have a lower risk for inducing EADs and other triggered activities and thus are more suitable to treat arrhythmias. If this hypothesis is correct, it suggests that the early assessment of cardiotoxicity risk could be improved by using in vitro ion channel assays that assess facilitation. Such an improvement could reduce the likelihood of mistakenly discarding viable drug candidates and speed the progression of safer drugs into clinical trials and clinical use.

Acknowledgments

We are grateful to Dr. Mark T. Keating and Dr. Michael C. Sanguinetti (University of Utah) for providing us with hERG clone; Dr. Craig T. January (University of Wisconsin) for providing us with HEK293 cell lines stably expressing hERG; Dr. Koichi Nakajo (Jichi Medical University) for providing us with rat KCNE2 clone; Benjamin Van, Dr. Julie Bossuyt, and Dr. Donald Bers (University of California, Davis) for providing rabbit ventricular myocytes; and Dr. Parashar Thapa (University of California, Davis) for help with blinding. We also thank Dr. Colleen Clancy and Dr. Eleonora Grandi (University of California, Davis) for discussion.

This study was supported by the Hiroshi and Aya Irisawa Memorial Promotion Award for Young Physiologists (K. Furutani and K. Tsumoto) from the Physiological Society of Japan; a Dean's Award from Department of Physiology and Membrane Biology, University of California, Davis (K. Furutani and J.T. Sack); Grants-in-Aid for the Scientific Research on Innovative Areas 22136002 (Y. Kurachi)15H01404 (K. Furutani) from the Ministry of Education, Science, Sports and Culture of Japan; Grants-in-Aid for the Scientific Research (C) 15K08231 (K. Furutani) and 16KT0194 (K. Tsumoto) from the Japan Society for the Promotion of Science; and National Institutes of Health grants U01HL126273 and R01HL128537 (K. Furutani and J.T. Sack).

The authors declare no competing financial interests.

Author contributions: K. Furutani and K. Tsumoto designed the experiments, conducted the experiments, analyzed the data, made figures, and wrote the manuscript. I-S. Chen conducted the experiments and wrote the manuscript. K. Handa and Y. Yamakawa conducted the experiments and revised the manuscript. J.T. Sack and Y. Kurachi supervised the project and wrote the manuscript.

Richard W. Aldrich served as editor.

Submitted: 30 July 2018
Accepted: 6 December 2018

References

Abbott, G.W., F. Sesti, I. Splawski, M.E. Buck, M.H. Lehmann, K.W. Timothy, M.T. Keating, and S.A. Goldstein. 1999. MiRP1 forms IKr potassium channels with HERG and is associated with cardiac arrhythmia. *Cell.* 97:175–187. https://doi.org/10.1016/S0092-8674(00)80728-X

Aiba, T., W. Shimizu, M. Inagaki, T. Noda, S. Miyoshi, W.G. Ding, D.P. Zankov, F. Toyoda, H. Matsuura, M. Horie, and K. Sunagawa. 2005. Cellular and ionic mechanism for drug-induced long QT syndrome and effectiveness of verapamil. *J. Am. Coll. Cardiol.* 45:300–307. https://doi.org/10.1016/j.jacc.2004.09.069

Asai, Y., T. Abe, H. Oka, M. Okita, T. Okuyama, K. Hagihara, S. Ghosh, Y. Matsuoka, Y. Kurachi, and H. Kitano. 2013. A versatile platform for multilevel modeling of physiological systems: template/instance framework for large-scale modeling and simulation. *Conf. Proc. IEEE Eng. Med. Biol. Soc.* 2013:5529–5532. https://doi.org/10.1109/EMBC.2013.6610802

Bayer, J.D., S.M. Narayan, G.G. Lalani, and N.A. Trayanova. 2010. Rate-dependent action potential alternans in human heart failure implicates abnormal intracellular calcium handling. *Heart Rhythm.* 7:1093–1101. https://doi.org/10.1016/j.hrthm.2010.04.008

Brendorp, B., H. Elming, L. Jun, L. Køber, and C. Torp-Pedersen. DIAMOND Study Group. Danish Investigations Of Arrhythmia and Mortality On Dofetilide. 2002. Effect of dofetilide on QT dispersion and the prognostic implications of changes in QT dispersion for patients with congestive heart failure. *Eur. J. Heart Fail.* 4:201–206. https://doi.org/10.1016/S1388-9842(01)00235-5

Carmeliet, E. 1993. Use-dependent block and use-dependent unblock of the delayed rectifier K+ current by almokalant in rabbit ventricular myocytes. *Circ. Res.* 73:857–868. https://doi.org/10.1161/01.RES.73.5.857

Cheng, J., K. Kamiya, I. Kodama, and J. Toyama. 1996. Differential effects of MS-551 and E-4031 on action potentials and the delayed rectifier K+ current in rabbit ventricular myocytes. *Cardiovasc. Res.* 31:963–974. https://doi.org/10.1016/S0008-6363(96)00049-1

Choi, B.R., F. Burton, and G. Salama. 2002. Cytosolic Ca2+ triggers early afterdepolarizations and Torsade de Pointes in rabbit hearts with type 2 long QT syndrome. *J. Physiol.* 543:615–631. https://doi.org/10.1113/jphysiol.2002.024570

Clancy, C.E., J. Kurokawa, M. Tateyama, X.H. Wehrens, and R.S. Kass. 2003. K+ channel structure-activity relationships and mechanisms of drug-induced QT prolongation. *Annu. Rev. Pharmacol. Toxicol.* 43:441–461. https://doi.org/10.1146/annurev.pharmtox.43.100901.140245

De Ponti, F., E. Poluzzi, and N. Montanaro. 2001. Organising evidence on QT prolongation and occurrence of Torsades de Pointes with non-antiarrhythmic drugs: a call for consensus. *Eur. J. Clin. Pharmacol.* 57:185–209. https://doi.org/10.1007/s002280100290

Drew, B.J., M.J. Ackerman, M. Funk, W.B. Gibler, P. Kligfield, V. Menon, G.J. Philippides, D.M. Roden, and W. Zareba. American Heart Association Acute Cardiac Care Committee of the Council on Clinical Cardiology, the Council on Cardiovascular Nursing, and the American College of Cardiology Foundation. 2010. Prevention of torsade de pointes in hospital settings: a scientific statement from the American Heart Association and the American College of Cardiology Foundation. *Circulation.* 121:1047–1060. https://doi.org/10.1161/CIRCULATIONAHA.109.192704

Drouin, E., F. Charpentier, C. Gauthier, K. Laurent, and H. Le Marec. 1995. Electrophysiologic characteristics of cells spanning the left ventricular wall of human heart: evidence for presence of M cells. *J. Am. Coll. Cardiol.* 26:185–192. https://doi.org/10.1016/0735-1097(95)00167-X

Elshrif, M.M., P. Shi, and E.M. Cherry. 2015. Representing variability and transmural differences in a model of human heart failure. *IEEE J. Biomed. Health Inform.* 19:1308–1320. https://doi.org/10.1109/JBHI.2015.2442833

Faber G.M., and Y. Rudy. 2000. Action potential and contractility changes in [Na(+)](i) overloaded cardiac myocytes: a simulation study. Biophys. J. 78:2392–2404. doi:, 1300828. https://doi.org/10.1016/S0006-3495(00)76783-X

Furutani, K., Y. Yamakawa, A. Inanobe, M. Iwata, Y. Ohno, and Y. Kurachi. 2011. A mechanism underlying compound-induced voltage shift in the current activation of hERG by antiarrhythmic agents. *Biochem. Biophys. Res. Commun.* 415:141–146. https://doi.org/10.1016/j.bbrc.2011.10.034

Gessner, G., R. Macianskiene, J.G. Starkus, R. Schönherr, and S.H. Heinemann. 2010. The amiodarone derivative KB130015 activates hERG1 potassium channels via a novel mechanism. *Eur. J. Pharmacol.* 632:52–59. https://doi.org/10.1016/j.ejphar.2010.01.010

Gintant, G., P.T. Sager, and N. Stockbridge. 2016. Evolution of strategies to improve preclinical cardiac safety testing. *Nat. Rev. Drug Discov.* 15:457–471. https://doi.org/10.1038/nrd.2015.34

Guo, D., Q. Liu, T. Liu, G. Elliott, M. Gingras, P.R. Kowey, and G.X. Yan. 2011. Electrophysiological properties of HBI-3000: a new antiarrhythmic agent with multiple-channel blocking properties in human ventricular myocytes. *J. Cardiovasc. Pharmacol.* 57:79–85. https://doi.org/10.1097/FJC.0b013e3181ffe8b3

Hafner, D., F. Berger, U. Borchard, A. Kullmann, and A. Scherlitz. 1988. Electrophysiological characterization of the class III activity of sotalol and its enantiomers. New interpretation of use-dependent effects. *Arzneimittelforschung.* 38:231–236.

Hamill, O.P., A. Marty, E. Neher, B. Sakmann, and F.J. Sigworth. 1981. Improved patch-clamp techniques for high-resolution current recording from cells and cell-free membrane patches. *Pflugers Arch.* 391:85–100. https://doi.org/10.1007/BF00656997

Hondeghem, L.M., and D.J. Snyders. 1990. Class III antiarrhythmic agents have a lot of potential but a long way to go. Reduced effectiveness and dangers of reverse use dependence. *Circulation.* 81:686–690. https://doi.org/10.1161/01.CIR.81.2.686

Hosaka, Y., M. Iwata, N. Kamiya, M. Yamada, K. Kinoshita, Y. Fukunishi, K. Tsujimae, H. Hibino, Y. Aizawa, A. Inanobe, et al. 2007. Mutational analysis of block and facilitation of HERG current by a class III anti-arrhythmic agent, nifekalant. *Channels (Austin).* 1:198–208. https://doi.org/10.4161/chan.4691

ICH. 2005. The non-clinical evaluation of the potential for delayed ventricular repolarization (QT interval prolongation) by human pharmaceuticals. Guidance on S7B. http://www.ich.org/products/guidelines/safety/safety-single/article/the-non-clinical-evaluation-of-the-potential-for-delayed-ventricular-repolarization-qt-interval-pro.html.

Igawa, M., K. Aonuma, Y. Okamoto, M. Hiroe, M. Hiraoka, and M. Isobe. 2002. Anti-arrhythmic efficacy of nifekalant hydrochloride, a pure class III anti-arrhythmic agent, in patients with healed myocardial infarction and inducible sustained ventricular tachycardia. *J. Cardiovasc. Pharmacol.* 40:735–742. https://doi.org/10.1097/00005344-200211000-00011

Jaiswal, A., and S. Goldbarg. 2014. Dofetilide induced torsade de pointes: mechanism, risk factors and management strategies. *Indian Heart J.* 66:640–648. https://doi.org/10.1016/j.ihj.2013.12.021

Jiang, M., W. Dun, J.S. Fan, and G.N. Tseng. 1999. Use-dependent 'agonist' effect of azimilide on the HERG channel. *J. Pharmacol. Exp. Ther.* 291:1324–1336.

Jost, N., L. Virág, M. Bitay, J. Takács, C. Lengyel, P. Biliczki, Z. Nagy, G. Bogáts, D.A. Lathrop, J.G. Papp, and A. Varró. 2005. Restricting excessive cardiac action potential and QT prolongation: a vital role for IKs in human ventricular muscle. *Circulation.* 112:1392–1399. https://doi.org/10.1161/CIRCULATIONAHA.105.550111

Jurkiewicz, N.K., and M.C. Sanguinetti. 1993. Rate-dependent prolongation of cardiac action potentials by a methanesulfonanilide class III antiarrhythmic agent. Specific block of rapidly activating delayed rectifier K+ current by dofetilide. *Circ. Res.* 72:75–83. https://doi.org/10.1161/01.RES.72.1.75

Konarzewska, H., G.A. Peeters, and M.C. Sanguinetti. 1995. Repolarizing K+ currents in nonfailing human hearts. Similarities between right septal subendocardial and left subepicardial ventricular myocytes. *Circulation.* 92:1179–1187. https://doi.org/10.1161/01.CIR.92.5.1179

Kramer, J., C.A. Obejero-Paz, G. Myatt, Y.A. Kuryshev, A. Bruening-Wright, J.S. Verducci, and A.M. Brown. 2013. MICE models: superior to the HERG model in predicting Torsade de Pointes. *Sci. Rep.* 3:2100. https://doi.org/10.1038/srep02100

Maruyama, M., S.F. Lin, Y. Xie, S.K. Chua, B. Joung, S. Han, T. Shinohara, M.J. Shen, Z. Qu, J.N. Weiss, and P.S. Chen. 2011. Genesis of phase 3 early afterdepolarizations and triggered activity in acquired long-QT syndrome. *Circ Arrhythm Electrophysiol.* 4:103–111. https://doi.org/10.1161/CIRCEP.110.959064

Mirams, G.R., Y. Cui, A. Sher, M. Fink, J. Cooper, B.M. Heath, N.C. McMahon, D.J. Gavaghan, and D. Noble. 2011. Simulation of multiple ion channel block provides improved early prediction of compounds' clinical torsadogenic risk. *Cardiovasc. Res.* 91:53–61. https://doi.org/10.1093/cvr/cvr044

Näbauer, M., D.J. Beuckelmann, P. Uberfuhr, and G. Steinbeck. 1996. Regional differences in current density and rate-dependent properties of the transient outward current in subepicardial and subendocardial myocytes of human left ventricle. *Circulation.* 93:168–177. https://doi.org/10.1161/01.CIR.93.1.168

Nakaya, H., N. Tohse, Y. Takeda, and M. Kanno. 1993. Effects of MS-551, a new class III antiarrhythmic drug, on action potential and membrane currents in rabbit ventricular myocytes. *Br. J. Pharmacol.* 109:157–163. https://doi.org/10.1111/j.1476-5381.1993.tb13546.x

Nalos, L., R. Varkevisser, M.K. Jonsson, M.J. Houtman, J.D. Beekman, R. van der Nagel, M.B. Thomsen, G. Duker, P. Sartipy, T.P. de Boer, et al. 2012. Comparison of the IKr blockers moxifloxacin, dofetilide and E-4031 in five screening models of pro-arrhythmia reveals lack of specificity of isolated cardiomyocytes. *Br. J. Pharmacol.* 165:467–478. https://doi.org/10.1111/j.1476-5381.2011.01558.x

Nattel, S., A. Maguy, S. Le Bouter, and Y.H. Yeh. 2007. Arrhythmogenic ion-channel remodeling in the heart: heart failure, myocardial infarction, and atrial fibrillation. *Physiol. Rev.* 87:425–456. https://doi.org/10.1152/physrev.00014.2006

O'Hara, T., L. Virág, A. Varró, and Y. Rudy. 2011. Simulation of the undiseased human cardiac ventricular action potential: model formulation and experimental validation. *PLOS Comput. Biol.* 7:e1002061. https://doi.org/10.1371/journal.pcbi.1002061

Okada, Y., S. Ogawa, T. Sadanaga, and H. Mitamura. 1996. Assessment of reverse use-dependent blocking actions of class III antiarrhythmic drugs by 24-hour Holter electrocardiography. *J. Am. Coll. Cardiol.* 27:84–89. https://doi.org/10.1016/0735-1097(95)00424-6

Redfern, W.S., L. Carlsson, A.S. Davis, W.G. Lynch, I. MacKenzie, S. Palethorpe, P.K.S. Siegl, I. Strang, A.T. Sullivan, R. Wallis, et al. 2003. Relationships between preclinical cardiac electrophysiology, clinical QT interval prolongation and torsade de pointes for a broad range of drugs: evidence for a provisional safety margin in drug development. *Cardiovasc. Res.* 58:32–45. https://doi.org/10.1016/S0008-6363(02)00846-5

Roden, D.M. 2000. Acquired long QT syndromes and the risk of proarrhythmia. *J. Cardiovasc. Electrophysiol.* 11:938–940. https://doi.org/10.1111/j.1540-8167.2000.tb00077.x

Roden, D.M. 2008. Cellular basis of drug-induced torsades de pointes. *Br. J. Pharmacol.* 154:1502–1507. https://doi.org/10.1038/bjp.2008.238

Sager, P.T., G. Gintant, J.R. Turner, S. Pettit, and N. Stockbridge. 2014. Rechanneling the cardiac proarrhythmia safety paradigm: a meeting report from the Cardiac Safety Research Consortium. *Am. Heart J.* 167:292–300. https://doi.org/10.1016/j.ahj.2013.11.004

Sanguinetti, M.C., and N.K. Jurkiewicz. 1990. Two components of cardiac delayed rectifier K+ current. Differential sensitivity to block by class III antiarrhythmic agents. *J. Gen. Physiol.* 96:195–215. https://doi.org/10.1085/jgp.96.1.195

Sanguinetti, M.C., and M. Tristani-Firouzi. 2006. hERG potassium channels and cardiac arrhythmia. *Nature.* 440:463–469. https://doi.org/10.1038/nature04710

Sanguinetti, M.C., C. Jiang, M.E. Curran, and M.T. Keating. 1995. A mechanistic link between an inherited and an acquired cardiac arrhythmia: HERG encodes the IKr potassium channel. *Cell.* 81:299–307. https://doi.org/10.1016/0092-8674(95)90340-2

Sato, D., L.H. Xie, T.P. Nguyen, J.N. Weiss, and Z. Qu. 2010. Irregularly appearing early afterdepolarizations in cardiac myocytes: random fluctuations or dynamical chaos? *Biophys. J.* 99:765–773. https://doi.org/10.1016/j.bpj.2010.05.019

Sato, S., Y. Zamami, T. Imai, S. Tanaka, T. Koyama, T. Niimura, M. Chuma, T. Koga, K. Takechi, Y. Kurata, et al. 2017. Meta-analysis of the efficacies of amiodarone and nifekalant in shock-resistant ventricular fibrillation and pulseless ventricular tachycardia. *Sci. Rep.* 7:12683. https://doi.org/10.1038/s41598-017-13073-0

Satoh, Y., A. Sugiyama, A. Takahara, K. Chiba, and K. Hashimoto. 2004. Electropharmacological and proarrhythmic effects of a class III antiarrhythmic drug nifekalant hydrochloride assessed using the in vivo canine models. *J. Cardiovasc. Pharmacol.* 43:715–723. https://doi.org/10.1097/00005344-200405000-00015

Studenik, C.R., Z. Zhou, and C.T. January. 2001. Differences in action potential and early afterdepolarization properties in LQT2 and LQT3 models of long QT syndrome. *Br. J. Pharmacol.* 132:85–92. https://doi.org/10.1038/sj.bjp.0703770

Sugiyama, A. 2008. Sensitive and reliable proarrhythmia in vivo animal models for predicting drug-induced torsades de pointes in patients with remodelled hearts. *Br. J. Pharmacol.* 154:1528–1537. https://doi.org/10.1038/bjp.2008.240

Surawicz, B. 1989. Electrophysiologic substrate of torsade de pointes: dispersion of repolarization or early afterdepolarizations? *J. Am. Coll. Cardiol.* 14:172–184. https://doi.org/10.1016/0735-1097(89)90069-7

Szabó, G., N. Szentandrássy, T. Bíró, B.I. Tóth, G. Czifra, J. Magyar, T. Bányász, A. Varró, L. Kovács, and P.P. Nánási. 2005. Asymmetrical distribution of ion channels in canine and human left-ventricular wall: epicardium versus midmyocardium. *Pflugers Arch.* 450:307–316. https://doi.org/10.1007/s00424-005-1445-z

Takenaka, K., S. Yasuda, S. Miyazaki, T. Kurita, Y. Sutani, I. Morii, S. Daikoku, S. Kamakura, and H. Nonogi. 2001. Initial experience with nifekalant hydrochloride (MS-551), a novel class III antiarrhythmic agent, in patients with acute extensive infarction and severe ventricular dysfunction. *Jpn. Circ. J.* 65:60–62. https://doi.org/10.1253/jcj.65.60

Tamargo, J., J.Y. Le Heuzey, and P. Mabo. 2015. Narrow therapeutic index drugs: a clinical pharmacological consideration to flecainide. *Eur. J. Clin. Pharmacol.* 71:549–567. https://doi.org/10.1007/s00228-015-1832-0

Tande, P.M., H. Bjørnstad, T. Yang, and H. Refsum. 1990. Rate-dependent class III antiarrhythmic action, negative chronotropy, and positive inotropy of a novel Ik blocking drug, UK-68,798: potent in guinea pig but no effect in rat myocardium. *J. Cardiovasc. Pharmacol.* 16:401–410. https://doi.org/10.1097/00005344-199009000-00008

ten Tusscher, K.H., and A.V. Panfilov. 2006. Alternans and spiral breakup in a human ventricular tissue model. *Am. J. Physiol. Heart Circ. Physiol.* 291:H1088–H1100. https://doi.org/10.1152/ajpheart.00109.2006

ten Tusscher, K.H., D. Noble, P.J. Noble, and A.V. Panfilov. 2004. A model for human ventricular tissue. *Am. J. Physiol. Heart Circ. Physiol.* 286:H1573–H1589. https://doi.org/10.1152/ajpheart.00794.2003

Thomsen, M.B., P.G. Volders, M. Stengl, R.L. Spätjens, J.D. Beekman, U. Bischoff, M.A. Kall, K. Frederiksen, J. Matz, and M.A. Vos. 2003. Electrophysiological safety of sertindole in dogs with normal and remodeled hearts. *J. Pharmacol. Exp. Ther.* 307:776–784. https://doi.org/10.1124/jpet.103.052753

Torp-Pedersen, C., M. Møller, P.E. Bloch-Thomsen, L. Køber, E. Sandøe, K. Egstrup, E. Agner, J. Carlsen, J. Videbaek, B. Marchant, and A.J. Camm. Danish Investigations of Arrhythmia and Mortality on Dofetilide Study Group. 1999. Dofetilide in patients with congestive heart failure and left ventricular dysfunction. *N. Engl. J. Med.* 341:857–865. https://doi.org/10.1056/NEJM199909163411201

Toyama, J., K. Kamiya, J. Cheng, J.K. Lee, R. Suzuki, and I. Kodama. 1997. Vesnarinone prolongs action potential duration without reverse frequency dependence in rabbit ventricular muscle by blocking the delayed rectifier K+ current. *Circulation.* 96:3696–3703. https://doi.org/10.1161/01.CIR.96.10.3696

Trudeau, M.C., J.W. Warmke, B. Ganetzky, and G.A. Robertson. 1995. HERG, a human inward rectifier in the voltage-gated potassium channel family. *Science.* 269:92–95. https://doi.org/10.1126/science.7604285

Tsumoto, K., Y. Kurata, K. Furutani, and Y. Kurachi. 2017. Hysteretic Dynamics of Multi-Stable Early Afterdepolarisations with Repolarisation Reserve Attenuation: A Potential Dynamical Mechanism for Cardiac Arrhythmias. *Sci. Rep.* 7:10771. https://doi.org/10.1038/s41598-017-11355-1

Vandersickel, N., I.V. Kazbanov, A. Nuitermans, L.D. Weise, R. Pandit, and A.V. Panfilov. 2014. A study of early afterdepolarizations in a model for human ventricular tissue. *PLoS One.* 9:e84595. https://doi.org/10.1371/journal.pone.0084595

Vaughan Williams, E.M. 1992. Classifying antiarrhythmic actions: by facts or speculation. *J. Clin. Pharmacol.* 32:964–977. https://doi.org/10.1002/j.1552-4604.1992.tb03797.x

Weiss, J.N., A. Garfinkel, H.S. Karagueuzian, P.S. Chen, and Z. Qu. 2010. Early afterdepolarizations and cardiac arrhythmias. *Heart Rhythm.* 7:1891–1899. https://doi.org/10.1016/j.hrthm.2010.09.017

Wood, B.M., M. Simon, S. Galice, C.C. Alim, M. Ferrero, N.N. Pinna, D.M. Bers, and J. Bossuyt. 2018. Cardiac CaMKII activation promotes rapid translocation to its extra-dyadic targets. *J. Mol. Cell. Cardiol.* 125:18–28. https://doi.org/10.1016/j.yjmcc.2018.10.010

Xie, L.H., F. Chen, H.S. Karagueuzian, and J.N. Weiss. 2009. Oxidative-stress-induced afterdepolarizations and calmodulin kinase II signaling. *Circ. Res.* 104:79–86. https://doi.org/10.1161/CIRCRESAHA.108.183475

Xu, X., S.J. Rials, Y. Wu, J.J. Salata, T. Liu, D.B. Bharucha, R.A. Marinchak, and P.R. Kowey. 2001. Left ventricular hypertrophy decreases slowly but not rapidly activating delayed rectifier potassium currents of epicardial and endocardial myocytes in rabbits. *Circulation.* 103:1585–1590. https://doi.org/10.1161/01.CIR.103.11.1585

Yamakawa, Y., K. Furutani, A. Inanobe, Y. Ohno, and Y. Kurachi. 2012. Pharmacophore modeling for hERG channel facilitation. *Biochem. Biophys. Res. Commun.* 418:161–166. https://doi.org/10.1016/j.bbrc.2011.12.153

Zeng, J., and Y. Rudy. 1995. Early afterdepolarizations in cardiac myocytes: mechanism and rate dependence. *Biophys. J.* 68:949–964. https://doi.org/10.1016/S0006-3495(95)80271-7

Zeng, J., K.R. Laurita, D.S. Rosenbaum, and Y. Rudy. 1995. Two components of the delayed rectifier K+ current in ventricular myocytes of the guinea pig type. Theoretical formulation and their role in repolarization. *Circ. Res.* 77:140–152. https://doi.org/10.1161/01.RES.77.1.140

Zhao, Z., H. Wen, N. Fefelova, C. Allen, A. Baba, T. Matsuda, and L.H. Xie. 2012. Revisiting the ionic mechanisms of early afterdepolarizations in cardiomyocytes: predominant by Ca waves or Ca currents? *Am. J. Physiol. Heart Circ. Physiol.* 302:H1636–H1644. https://doi.org/10.1152/ajpheart.00742.2011

Zhou, Z., C. Studenik, and C.T. January. 1995. Mechanisms of early afterdepolarizations induced by block of IKr. *Circulation.* 92:I-435.

Zhou, Z., Q. Gong, B. Ye, Z. Fan, J.C. Makielski, G.A. Robertson, and C.T. January. 1998. Properties of HERG channels stably expressed in HEK 293 cells studied at physiological temperature. *Biophys. J.* 74:230–241. https://doi.org/10.1016/S0006-3495(98)77782-3